1 **Sac1 links phosphoinositide turnover to cryptococcal virulence**

2

3 Elizabeth A. Gaylord[1], Hau Lam Choy[1,2], Guohua Chen[1,3], Sydney L. Briner[1], and Tamara L. Doering[1,*]

4 [1]Department of Molecular Microbiology, Washington University School of Medicine, St. Louis, MO, USA

5 [2]Current position: L.E.K. Consulting, Boston, MA, USA

6 [3]Current position: Pfizer, Inc., Chesterfield, MO, USA

7 *Corresponding author: doering@wustl.edu

8

9 Running head: Sac1 links PI turnover to cryptococcal virulence

10

11

12 **KEYWORDS**

13 *Cryptococcus neoformans,* mycology, phosphoinositide, PI4P, phosphatase, Sac1, virulence

14

ABSTRACT

Cryptococcus neoformans is an environmentally-acquired fungal pathogen that causes over 140,000 deaths per year. Cryptococcal infection occurs when infectious particles are deposited into the lung, where they encounter host phagocytic cells. *C. neoformans* may be engulfed by these phagocytes, an important step of infection that leads to outcomes ranging from termination of infection to cryptococcal dissemination. To study this critical process, we screened approximately 4,700 cryptococcal gene deletion mutants for altered uptake, using primary mouse and human phagocytic cells. Among the hits of these two screens, we identified 93 mutants with perturbed uptake in both systems, as well as others with differences in uptake by only one cell type. We further screened the hits for changes in thickness of the capsule, a protective polysaccharide layer around the cell which is an important cryptococcal virulence factor. The combination of our three screens yielded 45 mutants, including one lacking the phosphatidylinositol-4-phosphate phosphatase Sac1. In this work, we implicate Sac1 in both host cell uptake and capsule production. We found that *sac1* mutants exhibit lipid trafficking defects, reductions in secretory system function, and changes in capsule size and composition. Many of these changes occur specifically in tissue culture media, highlighting the role of Sac1 phosphatase activity in responding to the stress of host-like conditions. Overall, these findings show how genome-scale screening can identify cellular factors that contribute to our understanding of cryptococcal biology and demonstrate the role of Sac1 in determining fungal virulence. (240/250)

IMPORTANCE

Cryptococcus neoformans is a fungal pathogen with significant impact on global health. Cryptococcal cells inhaled from the environment are deposited into the lungs, where they first contact the human immune system. The interaction between *C. neoformans* and host cells is critical because this step of infection can determine whether the fungal cells die or proliferate within the human host. Despite the importance of this stage of infection, we have limited knowledge of cryptococcal factors that influence its outcome. In this study, we identify cryptococcal genes that affect uptake by both human and mouse cells. We also identify mutants with altered capsule, a protective coating that surrounds the cells to shield them from the host immune system. Finally, we characterize the role of one gene, *SAC1*, in these processes. Overall, this study contributes to our understanding of how *C. neoformans* interacts with and protects itself from host cells. (147/150)

Abstract word count: 385

42 Text word count: 5250

43 **INTRODUCTION**

44 *Cryptococcus neoformans* is a fungal pathogen that causes significant mortality in immunocompromised individu-
45 als, particularly those with HIV/AIDS (1). Despite recent advances in healthcare access and treatments, cryptococcal men-
46 ingitis still leads to 19% of AIDS-related deaths (2). The interaction between *C. neoformans* and host phagocytes begins
47 when environmentally-acquired fungal cells are deposited in the lung. Subsequent phagocytosis may lead to fungal cell
48 death and termination of the infection. However, in some cases cryptococcal cells can withstand the pressures exerted by
49 phagocytes to survive and proliferate within phagolysosomes (3–6). In this scenario, engulfment of the yeast likely en-
50 hances cryptococcal dissemination from the lung to other sites (7). Due to the pivotal role of this initial phase of crypto-
51 coccal pathogenesis, extensive efforts have been devoted to studying the interactions of *C. neoformans* with host phago-
52 cytic cells.

53 *C. neoformans* produces multiple factors which modulate its interactions with host cells and thereby provide pro-
54 tection from phagocytosis. These include the cell wall and surrounding polysaccharide capsule, complex glycan-based
55 structures which change in size and composition in response to environmental conditions. Strains with perturbations of
56 these structures often exhibit increased uptake by phagocytic cells (8, 9), demonstrating the importance of capsule for
57 protecting against phagocytosis.

58 Various models have been used to interrogate cryptococcal-host interactions. These include invertebrate and ver-
59 tebrate animals, amoeba, and primary and immortalized cells (3, 10–16). Genetic screens based on libraries of mutant host
60 or fungal cells have identified gene products that modulate interactions of cryptococci with specific cell lines. In one ex-
61 ample, Chun and colleagues subjected cryptococcal cells to insertional mutagenesis and identified mutations that affected
62 their uptake by RAW264.7 macrophages (17). Srikanta et al. used RNA interference and high-throughput imaging to find
63 host regulatory genes which govern the interactions of *C. neoformans* with THP-1 cells and discovered 25 fungal-specific
64 regulators of phagocytosis (18). By applying high-throughput imaging to a *C. neoformans* gene deletion collection (19),
65 Santiago-Tirado et al. identified 56 fungal genes that affect uptake by THP-1 cells (9). A common strength of these studies
66 is the genetic tractability and accessibility of the immortalized cell lines used. However, such lines lack some features of
67 primary host cells (20–22), which may limit these approaches. Screens may also be constrained by the availability and size
68 of *Cryptococcus* mutant collections. For example, the last study cited screened a library of approximately 1,200 single gene

69 deletion mutants (9), whereas much larger libraries are currently available, increasing our power to identify novel pheno-
70 types.

71 This report incorporates several important departures from previous screens designed to elucidate *C. neoformans*-
72 host interactions. First, we screened a collection of 4,692 single gene deletion mutants, representing over eighty percent
73 of the non-essential genes in the cryptococcal genome. Second, we applied a flexible medium-throughput imaging method
74 that avoids pitfalls of earlier studies, such as difficulty distinguishing adherent versus internalized yeast cells (23). Third,
75 we screened using primary cells from both mouse (murine bone marrow-derived macrophages; BMDM) and human (mon-
76 ocyte-derived macrophages; HMDM), to take advantage of a model system while also examining the system of greatest
77 clinical interest. Finally, we reasoned that many of our hits would have altered capsules, so we further tested mutants that
78 demonstrated altered phagocytosis for changes in capsule thickness. Overall, we identified 45 deletion strains which ex-
79 hibited altered uptake in both systems as well as altered capsule size.

80 While it is known that capsule material traffics at least in part through the secretory pathway (24), few proteins
81 involved in this process have been characterized. To address this gap, we focused on mutants that might have aberrant
82 capsule trafficking. One critical process in the regulation of secretion is the subcellular distribution of phosphoinositides
83 (PI). Various cellular PI species are defined by the patterns of phosphorylation on their inositol head groups. These species
84 are maintained at distinct cellular compartments by kinases and phosphatases, which specifically and reversibly phosphor-
85 ylate and dephosphorylate inositol (25). In this way, PIs help define membrane identity and regulate membrane-protein
86 interactions (25), thus playing important roles in secretory trafficking (26, 27). We therefore were particularly interested
87 to note that one strain, which emerged as a hit in all three of our screens, lacks the gene *SAC1* (*CKF44_06080*). Sac1 is a
88 phosphatase that is highly conserved in eukaryotes and acts in phosphoinositide metabolism (28). Our observation that
89 cells lacking Sac1 are hypocapsular thus suggested that modulation of phosphoinositide turnover in the secretory pathway
90 influences capsule synthesis. Below we use biochemical, imaging, and molecular engineering approaches to establish the
91 mechanism of this interaction, linking alterations in lipid homeostasis to the production of a critical cryptococcal virulence
92 factor.

93 **RESULTS**

94 <u>Fungal genes that influence interactions with host cells</u>

95 To identify fungal gene products that affect interactions with host cells, we screened 4,692 *C. neoformans* single
96 gene deletion mutants (19). In our assay, fungal cells were stained with Lucifer Yellow, opsonized with serum, and then
97 incubated with primary phagocytes to allow engulfment. The samples were washed to remove unassociated cells and then
98 stained with membrane-impermeant Calcofluor White to label externally-associated fungi and propidium iodide to label
99 phagocytic cell nuclei. We assessed fungal engulfment as the phagocytic index, or number of internalized fungi (stained
100 with Lucifer Yellow but not Calcofluor White) per host cell (identified by nuclear staining) (23). We define the uptake score
101 as the ratio of a mutant's phagocytic index to that of wild-type *C. neoformans* (KN99).

102 We first applied our assay to screen the interactions of *C. neoformans* with murine bone marrow-derived macro-
103 phages (BMDM), normalizing to fungal cell number to account for differences in mutant growth rates (Figure 1A). Because
104 these deletion library plates do not include WT control cells, we initially compared strain uptake scores to the median for
105 each plate and used permissive cutoffs to call roughly 10% of the strains as hits (Table S1A). We then subjected the 458
106 strains that we identified with increased or decreased uptake (Table S1B) to a second round of BMDM screening (Table
107 S1C), this time comparing them to in-plate wild-type controls and using more stringent cutoffs to select hits (Figure 1B;
108 Table S1D). In parallel, we screened them using human monocyte-derived macrophages (HMDM) in place of BMDM (Figure
109 1C; Tables S1E and S1F).

110 Our second round of screening narrowed the initial hits to 93 mutants that significantly influenced host interac-
111 tions in both BMDM and HMDM cells (Figure 1A, overlap of red and blue circles; Table S1G). When we applied Gene
112 Ontology (GO) analysis to the corresponding genes, we found that genes encoding cellular factors related to cytoskeletal
113 interactions and intracellular protein localization and transport, among other categories, were particularly enriched rela-
114 tive to their abundance in the genome (Figure 1D; see Discussion).

115 <u>Mutants with altered host interactions and capsule size</u>

116 We were particularly interested in gene products that might act in capsule production, because of the many out-
117 standing questions that remain about this process (29). As the outermost layer of the cell, the capsule is fundamental in
118 mediating cryptococcal interactions (7). Therefore, we hypothesized that our uptake screen hits would be enriched for
119 mutants with altered capsule. To test this idea, we adapted an automated, fluorescence-based capsule quantification assay
120 (30) to accommodate medium-throughput screening. Of the 458 first round hits from the uptake screen, 131 indeed
121 showed capsule changes (Figure 1A), with 57 strains identified as hypocapsular and 74 as hypercapsular (Figure 1E; Tables

122 S2A, 2B). Validating the screen, this group contained multiple previously-identified capsule mutants, including 16 that were
123 hypocapsular and 3 that were hypercapsular. GO terms for the hits were particularly enriched for roles in capsule organi-
124 zation, as we expected, and for processes related to vesicular traffic, some of which were also enriched in our uptake
125 screen hits. Uniquely enriched for the capsule screen hits were ion transport and phosphoinositide binding (Figure 1F).

126 We identified 45 mutants which were hits in all three of our screens (Table S2C). The combination of perturbed
127 interactions with phagocytes and altered capsule thickness of these strains suggested that the deleted genes would be
128 important for virulence. We further speculated that the uptake phenotypes were related to surface changes in the cells,
129 which might be mechanistically elucidated by analysis of the deleted genes. Of the 45 triple hits, 18 had been previously
130 characterized. When we used homology to predict the subcellular localization of the remaining gene products, the largest
131 group (8 of 27) was predicted to reside in the secretory pathway. We suspected these genes might influence secretion of
132 capsule material.

133 Among the eight mutants likely impaired in secretion, we particularly noticed one strain that showed increased
134 phagocytosis by both BMDM and HMDM and a 61% reduction in capsule thickness compared to WT cells (Figure 2A). Its
135 missing sequence, *CKF44_06080*, encodes a protein with 38% amino acid identity to the phosphatidylinositol phosphatase
136 Sac1 of *Saccharomyces cerevisiae,* including 85% identity across a 20-amino acid region that encodes a conserved $CX_5R(RT)$
137 motif necessary for catalytic function (31). Interestingly, despite this similarity, ectopic overexpression of *S. cerevisiae* Sac1
138 did not restore the capsule defects of *sac1*Δ cells (Figure S1).

139 The phenotypes of *sac1*Δ cells, together with the unique biology of the capsule and its importance as a virulence
140 factor, led us to further investigate the role of Sac1 in *C. neoformans*. To pursue these studies, we first engineered a new
141 Sac1 deletion strain (*sac1*Δ) and complemented the mutant at the endogenous site (*SAC1*). We also identified the con-
142 served Sac1 catalytic motif by homology to *S. cerevisiae* Sac1 and inactivated it by replacing an aspartic acid residue with
143 alanine ($SAC1^{456A}$, Figure 2B and S2) (32, 33). Using these strains, we confirmed that loss of Sac1 led to thinner capsules, a
144 phenotype which was maintained after normalization to the smaller diameters of the *sac1*Δ cells (Figure 2C, D). These
145 traits were phenocopied by the inactivated strain, showing that the phosphatase function of Sac1 is essential for capsule
146 production, while complementation restored WT phenotypes (Figure 2C, D). While imaging, we also observed striking
147 round structures in the *sac1* mutant cells (Figure 2C, right panels). These were distinguished from typical organelles, like
148 the vacuoles visible in WT and *SAC1* cells, by their circular shape, defined edge, and striking refractility and only occurred

149 in *sac1* mutants grown in host-like conditions (here defined as DMEM, 37°C, 5% CO_2). These structures will be further
150 discussed below.

151 Sac1 is required for cryptococcal virulence

152 Variations in both uptake and capsule size are associated with changes in pathogenicity (9, 34–40), so we suspected
153 that *sac*1 mutants would have impaired virulence. To test this, we infected mice intranasally and measured organ burden
154 at 14 days post-infection. Notably, while *sac1*Δ cells were recovered from the lungs, they remained close to the level of the
155 original inoculum. In sharp contrast, the lung burden of WT and *SAC1* infected animals increased roughly 2000-fold in this
156 period (Figure 3A). Cells were recovered from the brain in only a minority of mutant infections, although all WT-infected
157 animals had detectable brain burden by this time point (Figure 3B). We observed similar results in a time course study,
158 which demonstrated gradual accumulation of cryptococci in the lung up to 18 days post-infection (Figure S3A) and impaired
159 dissemination to the brain (Figure S3B). These results motivated us to define the mechanism(s) by which Sac1 influences
160 virulence.

161 Sac1 controls substrate distribution and sensitivity to stressors

162 Sac1 has not been characterized in *C. neoformans.* To test its influence on turnover of intracellular PI4P, we engi-
163 neered strains to express an mNeonGreen-tagged peptide that binds PI4P (FAPP1) and has been used to assess its locali-
164 zation (41). We then examined the abundance and localization of this fluorescent peptide (Figure 4A). Overall, the FAPP1
165 signal was brighter in *sac1*Δ cells than in WT, a trend supported by flow cytometry (Figure S4). This is consistent with a role
166 for Sac1 as a PI4P phosphatase, as loss of this protein would lead to an increase in its substrate. We also noted distinctive
167 bright perinuclear rings in the *sac1*Δ cells (especially in rich medium), which were more diffuse in WT cells. These corre-
168 spond to an endoplasmic reticulum distribution (42) and suggest aberrant accumulation of PI4P in the early secretory
169 pathway. Finally, the mutant strain exhibited intense puncta, absent from WT cells, which are consistent with PI4P accu-
170 mulation in the yeast Golgi (43).

171 Secretion is a vital cellular process, so its perturbation could have multiple deleterious effects on the cell, including
172 effects on the plasma membrane and cell wall. To examine this, we tested strain growth in various stressful conditions.
173 Although both *sac1* mutants grow slightly slower than WT or complemented cells even on rich medium, they showed much
174 worse growth on media containing membrane stressors (the detergent SDS and the sterol-binding antifungal amphotericin

175 B) or the cell wall stressor Congo Red (Figure 4B). These defects were exacerbated when cells were grown at 37°C. In all of
176 our assays, the complemented strain phenocopied WT and the inactivated construct phenocopied the deletion mutant.

177 Sac1 regulates cellular lipids during the response to host-like conditions

178 We sought to explain the capsule defect and stress sensitivities of *sac1* mutants based on the cellular conse-
179 quences of perturbed PI4P turnover. In other eukaryotes, PI4P is important for establishing the lipid composition of secre-
180 tory vesicles (44) and its turnover is critical for the progression of post-Golgi secretory traffic (45). We therefore examined
181 classes of molecules, including lipids, proteins, and capsule polysaccharides, that are directly or indirectly influenced by
182 this step of secretion. As noted above, we had observed formation of large internal structures in *sac1* mutant cells grown
183 under host-like conditions (Figure 2C), which were absent from WT and complemented cells. Because of their shape and
184 refractile appearance in light micrographs, we suspected they were at least in part composed of lipid. Consistent with this
185 suggestion, they appeared electron-lucent by transmission electron microscopy (Figure 5A, asterisks). We hypothesized
186 that these structures result from aberrant lipid handling within *sac1* mutant cells that is induced by the stress of host-like
187 conditions, since they are absent from mutant cells grown in rich medium (Figure 5A). Based on this idea, and our results
188 below, we termed them Sac1 lipid-accumulating bodies (SLBs).

189 SLBs resemble previously-characterized ”supersized” lipid droplets identified in *S. cerevisiae* (46). Lipid droplets
190 are neutral lipid-containing structures that represent essential cellular energy reserves; these increase in abundance when
191 cryptococcal cells are grown in host-like conditions (47). When we stained for neutral lipids using Nile Red, WT cryptococcal
192 cells showed dispersed punctate signal, while *sac1Δ* cells showed concentrated central staining, frequently colocalized
193 with SLBs (Figure 5B,C) and thus supporting the presence of neutral lipids within them.

194 We recently demonstrated that mislocalization of the important fungal lipid ergosterol leads to accumulation of
195 lipid droplets (47). We had also noted that *sac1* mutants were more sensitive than WT cells to Amphotericin B, which binds
196 ergosterol (Figure 4B). Consequently, we wondered whether ergosterol localization in *sac1*Δ cells was perturbed. When
197 we stained WT cells grown in host-like conditions with filipin, which binds non-esterified sterols, we saw the typical ring-
198 staining expected for a component of the plasma membrane (Figure 5D). By contrast, mutant cells exhibited increased
199 internal staining, particularly bordering the SLBs (see Discussion). When we tested filipin and Nile Red together, both stains
200 localized to SLBs in the *sac1* mutants, with a ring of filipin surrounding the Nile Red stain (Figure S5). In contrast, WT cells
201 showed peripheral filipin staining and Nile Red staining dispersed throughout the cell.

202 In testing cell growth, we fortuitously discovered that supplementation of host-like conditions (DMEM, 37°C, 5%
203 CO_2) with various exogenous fatty acids partially restored the growth of *sac1*Δ cells (Figure 6 and Supplemental Figure S6);
204 this effect was dose-dependent (shown for myristate in Figure 6A). This supplementation also prevented the formation of
205 SLBs (Figure 6B, bottom right panel). When we visualized capsule in myristate-supplemented cells, we made several ob-
206 servations. First, the addition of the BSA vehicle alone led to a slight capsule size increase, of similar magnitude, in both
207 cell types. Second, myristate supplementation yielded significant capsule reduction in both strains, which was more dra-
208 matic in the mutant (Figure 6B). Lipid supplementation thus restores growth and prevents SLAB formation in *sac1*Δ cells
209 but does not rescue capsule size (see Discussion).

210 Sac1 impacts protein secretion and localization

211 Proteins are critical secretory cargo, so it is likely that accumulation of PI4P in the secretory pathway would affect
212 their transport and secretion. To assess this, we measured protein secretion directly, using inducible acid phosphatase
213 production as a proxy for general protein secretion (24). Upon entry into phosphate-depleted conditions, WT, *SAC1*, and
214 both *sac1* mutants began producing detectable levels of acid phosphatase within one hour. While the general patterns of
215 secretion were similar, the mutants produced less acid phosphatase on a per cell basis throughout the time course (Figure
216 7A), suggesting an overall reduction in protein secretion.

217 Perturbations in PI4P levels may affect not only proteins secreted outside the cell, but also those resident in the
218 secretory system, including multiple capsule biosynthetic proteins in the Golgi apparatus. We hypothesized that the loss
219 of PI4P turnover could result in failure to correctly localize these enzymes and thereby explain the altered capsule of *sac1*
220 mutants. To investigate this question, we localized the best-characterized capsule biosynthetic enzyme, Cxt1 (48), in *sac1*Δ
221 and WT cells grown in host-like conditions. WT cells displayed clear puncta of Cxt1-mNeonGreen, consistent with the ex-
222 pected Golgi localization of this protein. In contrast, staining in *sac1*Δ cells was heterogenous, with various cell populations
223 displaying punctate, diffuse, or little to no fluorescence (Figure 7B, C).

224 Sac1 affects capsule secretion and composition

225 Capsule glycans constitute a class of secretory cargo which is unique to *C. neoformans*. The predominant capsule
226 polysaccharide, glucuronoxylomannan (GXM), traverses the secretory pathway prior to extracellular release (24). We hy-
227 pothesized that GXM secretion, like protein secretion, is reduced in *sac1*Δ cells, causing their thin capsules. To test this, we
228 quantified GXM secretion at intervals after transition to host-like conditions. Importantly, WT and *sac1* mutants began to

229 produce detectable levels of GXM concurrently, showing that the mutants respond normally to the environmental signals
230 that trigger capsule production (Figure 7D). However, the overall amount of GXM they secreted was markedly reduced.
231 Reduced GXM secretion could certainly explain the small capsules of *sac1* mutant cells. Another reason for altered
232 capsule could be mislocalization of glycosyltransferases (such as we observed with Cxt1), since compositional differences
233 in the polysaccharide also affect capsule size and architecture (8). To investigate this, we analyzed the composition of GXM
234 purified from WT, *sac1*Δ, and *SAC1* cells. Compared to the WT and *SAC1* controls, *sac1*Δ GXM showed a substantial (~2-
235 fold) increase in the relative proportion of glucuronic acid, as well as a modest increase in xylose (Figure 7E). These results
236 were supported by linkage analysis, in which we observed a reduction in 3-linked mannopyrannosyl residues as a fraction
237 of the total (Supplemental Table S3), indicating fewer unmodified backbone mannose residues.
238
239 **DISCUSSION**
240 How *C. neoformans* interacts with host cells is a critical determinant of infection. In this study, we screened 4,692
241 cryptococcal deletion strains and identified 93 that demonstrated altered uptake by both mouse and human primary phag-
242 ocytes. GO analysis showed that this set was enriched in sequences that encode proteins with roles in cytoskeletal inter-
243 actions, protein transport, and organization of the cell wall and capsule. This is consistent with our understanding that the
244 outer layers of the cell and secreted factors modulate interactions with host cells. We also identified strains with defects
245 in only one host system. Why the species differ in this regard could be a fruitful area for future research.
246 Capsule is a critical factor in the interaction between *C. neoformans* and host cells, but the mechanisms of its
247 synthesis and transport remain largely unknown. To approach this question, we performed a secondary screen for altered
248 capsule thickness, which yielded 131 mutants. For comparison, a previous screen of 1,201 deletion strains, using colony
249 morphology as the primary screen, yielded 16 capsule-related genes (19). Furthermore, our hits represent approximately
250 one third of the original set of uptake mutants that we tested. This shows that our strategy of using these mutants as the
251 starting population to screen for capsule defects was highly successful in enriching for capsule phenotypes. Notably, 42 of
252 the hits are annotated as encoding hypothetical proteins (49), which may be subjects for future investigation. The others
253 were enriched for GO terms related to cell wall and capsule organization, which validated our methods, and for terms
254 involving transporter activity, intracellular transport, and phosphatidylinositol binding. As our results with Sac1

255 demonstrate, the study of such processes, which are not directly related to capsule production, may still yield insight into
256 capsule biosynthesis.

257 Interestingly, over half of our capsule screen hits were hypercapsular strains. This highlights an important strength
258 of our image-based technique, as prior methods (including colony morphology, antibody blotting, or volume-based meth-
259 ods) identify strains that lack capsule more readily than hypercapsular cells (50). That said, image-based screens may also
260 have weaknesses. For example, mutants with general morphological defects may register as false positives, as cells that
261 fail to divide might appear to be one large cell with a capsule defect. Further, this method cannot identify mutants that are
262 completely acapsular, as they will not bind antibody.

263 Of the 45 gene products identified as hits in all three of our screens, the largest subset of the uncharacterized hits
264 was predicted to be involved in the secretory pathway. We focused on one of these hits, Sac1, a PI4P phosphatase encoded
265 by *CKF44_06080.* The *CNAG_06080* gene (which encodes Sac1 in the closely-related reference strain H99) was previously
266 identified as a site where random integration of a drug marker yielded an attenuated *C. neoformans* strain (51). Like our
267 KN99 mutant, this strain showed reduced virulence, although direct comparison is limited because the mutations, mouse
268 models, and experimental designs differ. Other investigators had proposed that this gene was essential, because they were
269 unable to delete it (52). We expect this difference from our findings was due to the challenge of working with cells that
270 have significant defects, although it could also reflect different strain backgrounds (H99S vs KN99) (53, 54).

271 By expressing and localizing a fluorescent PI4P-binding peptide (41, 55, 56), we supported a role for Sac1 in PI4P
272 turnover in *C. neoformans*. Although we did not test this activity directly, based on homology to the well-characterized *S.*
273 *cerevisiae* Sac1 protein, conservation of Sac1 function throughout eukaryotes, and our binding data, we believe PI4P is the
274 main substrate of Sac1 in *C. neoformans*. It is curious that despite its high amino acid similarity to the *S. cerevisiae* Sac1
275 protein, over-expression of the latter did not rescue the defects of *C. neoformans sac1*Δ cells; this result may warrant
276 further experimentation.

277 When s*ac1* mutants are grown in host-like medium, they develop large structures which we termed SLBs. The
278 interiors of SLBs stain with Nile Red, which binds neutral lipids, and the edges stain with the sterol-binding dye filipin. SLBS
279 thus share certain features with lipid droplets, which are composed of a neutral lipid core of mainly triacylglycerols and
280 sterol esters surrounded by a phospholipid monolayer (57). More specifically, SLBs resemble “supersized” lipid droplets,
281 which form in model yeast strains defective in phospholipid metabolism (46, 58). This phenomenon has also been observed

282 in *C. neoformans* following treatment with the antidepressant sertraline (59). However, our filipin staining suggests the
283 presence of ergosterol or sterol intermediates (60) on the perimeter of the SLBs, which has not been reported for regular
284 or supersized lipid droplets; accordingly we have not adopted this terminology.

285 Ergosterol is distributed in a steeply increasing gradient from the ER to the plasma membrane (61). One model
286 proposes that PI4P turnover by Sac1 maintains this gradient (62). If this mechanism occurs in *C. neoformans,* loss of PI4P
287 turnover would likely result in the inability to shuttle ergosterol up its concentration gradient with consequent accumula-
288 tion in the ER. Another model suggests that the ergosterol gradient depends on membrane phospholipid composition (61).
289 In either case, loss of Sac1 could perturb lipid transport and homeostasis and lead to mislocalization of ergosterol.

290 PI4P is a key signaling lipid, that serves as a pro-secretory marker and modulates the exit of secretory traffic from
291 the *trans*-Golgi (27, 44, 63). We propose that the lack of PI4P turnover in *sac1* mutants leads to its accumulation in the
292 early portions of the cryptococcal secretory system. This would be consistent with our observations of reduced protein
293 secretion and mislocalization of the Golgi-resident protein Cxt1 in *sac1*Δ cells. The Golgi serves as a central hub for traf-
294 ficking of both proteins and lipids, and in doing so plays a key role in membrane trafficking and lipid metabolism (64). We
295 hypothesize that SLAB formation in *sac1* mutants represents the failure of lipid trafficking under stressful, nutrient-limited
296 host-like conditions, leading to the accumulation of lipid cargo and/or lipid metabolic precursors. SLAB formation and the
297 poor growth of *sac1*Δ cells is prevented by fatty acid supplementation, which somehow bypasses the defect caused by
298 PI4P accumulation and allows the cells to grow normally. How this occurs will be an interesting question for future research.
299 Importantly, while fatty acid supplementation rescues SLAB formation in *sac1*Δ cells, capsule production is not restored.
300 This key finding shows that the adverse effects of Sac1 loss occur in divergent pathways.

301 Capsule material is exported in secretory vesicles (24), so defects in anterograde traffic would also impair this
302 process. Beyond reduced GXM secretion, which is consistent with this expectation, we observed alterations in GXM com-
303 position: the mannose backbone had a large increase in glucuronic acid substitution and a slight increase in xylose. We
304 hypothesize that altered localization of capsule biosynthetic enzymes changes their access to nascent capsule material and
305 precursor molecules. It is not known whether capsule polysaccharides traverse the cell as subunits or extended polymers
306 (65, 66), but in either case increased exposure to biosynthetic enzymes could result in compositional changes such as we
307 observed. Both the reduction of capsule size and changes in composition in *sac1* mutants likely contribute to their in-
308 creased uptake by host phagocytes.

309 In this study, we identified *C. neoformans* mutants impaired in host interactions with primary cells and assessed
310 the hits for capsule defects. This strategy greatly increased the number of sequences known to influence capsule produc-
311 tion, including many previously uncharacterized genes. Analysis of these genes and the corresponding mutants will help
312 us understand the processes required for synthesis of this central virulence factor, as exemplified in this work on Sac1.
313 Importantly, two-thirds of our original uptake hits did not have altered capsule thickness, implicating additional mecha-
314 nisms in this fundamental host-pathogen interaction. Further studies will be required to determine what leads to the al-
315 tered uptake of these strains, which may include changes to the cell wall or surface mannoproteins (29) or structural alter-
316 ations in the capsule that do not impact its thickness.
317

318 **METHODS**

319 Strain construction, validation, and growth

320 *sac1Δ*, *SAC1* complement, and *SAC1*^{D456A} strains were made with split-marker biolistic transformation (67) in
321 KN99α. Cxt1 was tagged with mNEONGREEN (pBHM2404, Addgene #173441, a gift from Hiten Madhani) using CRISPR
322 with short homology-directed repair (68). FAPP1-mNeonGreen (from pRS406-PHO5-GFP-hFAPP1_PH_domain, Addgene
323 #58723, a gift from Tim Levine) and *S. cerevisiae SAC1* strains were similarly inserted in the Safe Haven 2 region (68, 69).

324 Transformants were validated by antifungal resistance, PCR and/or whole genome sequencing. Expression of *S.*
325 *cerevisiae* S288C *SAC1* was confirmed by extracting total RNA with TRIzol Reagent, synthesizing cDNA using SuperScript III
326 (Thermo Fisher, #18080400), and PCR-amplifying a unique region of the gene (Fig. S1B).

327 For all assays except screening, *C. neoformans* strains were grown on YPD plates (2 days, 30°C) and single colonies
328 were inoculated into YPD and grown overnight (30°C, shaking). For capsule inductions, cells were washed in PBS, inocu-
329 lated in DMEM at 10^6 cells/mL, and grown for 16-24 hours (static, 37°C, 5% CO_2). For screening, cells were cultured from
330 glycerol stocks in 96-well plates, grown overnight in YPD, and then sub-cultured and grown 24 hours in YPD. Detailed
331 methods, including stress media and lipid supplementation, are in Supplemental Materials.

332 Screening

333 For uptake screening, C57BL/6J mouse BMDMs were harvested as in (70) and differentiated for 9 days before
334 isolation. HMDMs were from anonymous donors. PBMCs were isolated by Ficoll-Paque centrifugation and differentiated
335 for 6 days. The screen assay was modified from (23). Briefly, opsonized Lucifer Yellow-stained fungi were added to host

336 cells at an MOI of 20 (BMDM) or 30 (HMDM) and the cultures were co-incubated for one hour and washed. Adherent cells
337 were stained with Calcofluor White; wells were washed, fixed, and permeabilized; and host cell nuclei were stained with
338 propidium iodide before imaging on a BioTek Cytation 3. The uptake index (internalized cells per macrophage) was cor-
339 rected for the number of fungal cells added and then normalized to the plate median (first round) or KN99 value (later
340 rounds).

341 For capsule screening, strains identified as hits in the first round BMDM uptake screen were assessed for capsule
342 size differences using slight modifications of our previous method (30). For this, cells were induced as above, capsules
343 were stained with anti-GXM mAb-302-AF488, and cell walls were stained with Calcofluor White. Images were collected as
344 above, and capsule thickness measured as in (31).

345 Further details of methods and hit selection for both screens are in Supplemental Material.

346 Virulence studies

347 All animal protocols were approved by the Washington University Institutional Animal Care and Use Committee
348 (Protocol #20-0108) and care was taken to minimize animal handling and discomfort. 6-8-week-old female C57BL/6 mice
349 (The Jackson Laboratory) were anesthetized by subcutaneous injection of 1.20 mg ketamine and 0.24 mg xylazine in 110
350 µL sterile PBS. For 14-day infections, mice were intranasally infected with 5×10^4 cryptococcal cells. For time course infec-
351 tion, mice were infected with 1.25×10^4 cryptococcal cells and sacrificed at 6, 12, and 18-days post infection. For both
352 infections, the lungs and brains were harvested, homogenized, and plated on YPD agar to assess fungal organ burden.

353 Assays

354 Acid phosphatase secretion was measured as in (24). 10^7 cells/mL cultures were grown in MM-KCl (0.5% KCl, 15
355 mM glucose, 10 mM $MgSO_4 \cdot 7H_2O$, 13 mM glycine, 3.0 µM thiamine). Supernatants were sampled, incubated with sub-
356 strate buffer (2.5 mM para-nitrophenylphosphate in 50 mM acetate buffer, pH 4.0) at 37°C for 5 minutes, and stopped
357 with 800 µL saturated Na_2CO_3. Acid phosphatase secretion was quantified as A_{420}/OD_{600}.

358 GXM ELISAs were performed as in (48). Cultures were induced in DMEM,and the supernatants filtered (0.2 µm).
359 Flat-bottom Immulon 1B plates (Thermo Scientific) were coated with 1 µg/ml anti-GXM antibodies 339 and F12D2γ,
360 washed with PBS with 0.5% TWEEN 20 (PBST), and blocked for 90 min with 1% BSA in PBST. Filtrates were diluted in PBST
361 and incubated on the plate for 90 min. The plate was washed three times, probed with HRP-labeled mAb 339/F12D2γ,
362 incubated with KPL TMB Microwell Peroxidase Substrate (SeraCare), developed, and quantified using A_{450}.

363 Imaging

364 For capsule visualization, cells were induced as above, mixed with India ink in PBS (1:2, v:v), and imaged by light
365 microscopy. Capsules of at least 96 cells from randomly-chosen fields were measured using ImageJ. Nile Red and filipin
366 staining was performed as in (47), and viewed on a ZEISS Axio Imager M2 fluorescence microscope. FAPP1-mNEONGREEN
367 and Cxt1-mNEONGREEN stains were imaged with a Zeiss LSM880 confocal microscope. Morphological classification of
368 Cxt1-mNeonGreen and Nile Red staining was performed on at least 94 cells from randomly-selected fields. Electron mi-
369 croscopy was as in (47) with one change detailed in Supplement.

370 GXM analysis

371 GXM was isolated using precipitation with hexadecyltrimethylammonium bromide as in (71). Isolated material
372 was hydrolyzed with trifluoroacetic acid (3 hr, 100°C) and composition assessed on a Dionex ICS-6000 instrument. Linkage
373 analysis was performed by the Complex Carbohydrate Research Center (method modified from (72)).

374

375 **ACKNOWLEDGEMENTS**

376 We thank Nicole Howard and Suhas Bobba for assistance with host cells, Todd Fehniger and lab for LRS chambers
377 for HMDM isolation, Yan Xie for statistical analysis, Wandy Beatty for electron microscopy, and Tim Levine for plasmid
378 sequences. We appreciate the assistance of Jessica Tuck and Alex Caron with phenotypic characterization and microscopy
379 studies. We thank Doering lab members for discussions, and particularly Liza Loza, Daphne Boodwa-Ko, Thomas Hurtaux,
380 and Zanetta Chang for comments on the manuscript.

381 This work was supported by NIH grants AI140979, AI135012, and AI178330 to T.L.D. E.A.G and H.L.C were partially
382 supported by T32 GM007067, and E.A.G. by a Sondra Schlesinger Graduate Fellowship from the Department of Molecular
383 Microbiology, Washington University School of Medicine. The cryptococcal deletion library, developed by the Madhani lab
384 with funding from R01AI100272, was purchased from the Fungal Genetics Stock Center. The CCRC is supported by the U.S.
385 Department of Energy, Office of Science, Basic Energy Sciences, grant number DE-SC0015662 to Parastoo Azadi.

386

387 **REFERENCES**

388 1. Denning DW. 2024. Global incidence and mortality of severe fungal disease. Lancet Infect Dis
389 https://doi.org/10.1016/S1473-3099(23)00692-8.

390 2. Rajasingham R, Govender NP, Jordan A, Loyse A, Shroufi A, Denning DW, Meya DB, Chiller TM, Boulware DR. 2022.
391 The global burden of HIV-associated cryptococcal infection in adults in 2020: a modelling analysis. Lancet Infect Dis
392 22:1748–1755.

393 3. Feldmesser M, Kress Y, Novikoff P, Casadevall A. 2000. *Cryptococcus neoformans* is a facultative intracellular patho-
394 gen in murine pulmonary infection. Infect Immun 68:4225–4237.

395 4. Tucker SC, Casadevall A. 2002. Replication of *Cryptococcus neoformans* in macrophages is accompanied by phago-
396 somal permeabilization and accumulation of vesicles containing polysaccharide in the cytoplasm. Proc Natl Acad Sci
397 U S A 99:3165–3170.

398 5. Del Poeta M. 2004. Role of phagocytosis in the virulence of *Cryptococcus neoformans*. Eukaryot Cell 3:1067–1075.

399 6. Osterholzer JJ, Surana R, Milam JE, Montano GT, Chen G-H, Sonstein J, Curtis JL, Huffnagle GB, Toews GB, Olszewski
400 MA. 2009. Cryptococcal urease promotes the accumulation of immature dendritic cells and a non-protective T2
401 immune response within the lung. Am J Pathol 174:932–943.

402 7. Gaylord EA, Choy HL, Doering TL. 2020. Dangerous liaisons: Interactions of *Cryptococcus neoformans* with host
403 phagocytes. Pathog Basel Switz 9:891.

404 8. Li LX, Rautengarten C, Heazlewood JL, Doering TL. 2018. UDP-glucuronic acid transport is required for virulence of
405 *cryptococcus neoformans*. mBio 9:e02319-17.

406 9. Santiago-Tirado FH, Peng T, Yang M, Hang HC, Doering TL. 2015. A Single Protein S-acyl Transferase Acts through
407 Diverse Substrates to Determine Cryptococcal Morphology, Stress Tolerance, and Pathogenic Outcome. PLoS
408 Pathog 11.

409 10. Steenbergen JN, Shuman HA, Casadevall A. 2001. *Cryptococcus neoformans* interactions with amoebae suggest an
410 explanation for its virulence and intracellular pathogenic strategy in macrophages. Proc Natl Acad Sci 98:15245–
411 15250.

412 11. Mylonakis E, Moreno R, El Khoury JB, Idnurm A, Heitman J, Calderwood SB, Ausubel FM, Diener A. 2005. *Galleria*
413 *mellonella* as a model system to study *Cryptococcus neoformans* pathogenesis. Infect Immun 73:3842–3850.

414 12. Mukaremera L, McDonald TR, Nielsen JN, Molenaar CJ, Akampurira A, Schutz C, Taseera K, Muzoora C, Meintjes G,
415 Meya DB, Boulware DR, Nielsen K. 2019. The mouse inhalation model of *Cryptococcus neoformans* infection reca-
416 pitulates strain virulence in humans and shows that closely related strains can possess differential virulence. Infect
417 Immun 87:e00046-19.

418 13. Syme RM, Spurrell JCL, Amankwah EK, Green FHY, Mody CH. 2002. Primary dendritic cells phagocytose *Cryptococ-*
419 *cus neoformans* via mannose receptors and Fcγ receptor II for presentation to T lymphocytes. Infect Immun
420 70:5972–5981.

421 14. Alvarez M, Casadevall A. 2006. Phagosome extrusion and host-cell survival after *Cryptococcus neoformans* phagocy-
422 tosis by macrophages. Curr Biol 16:2161–2165.

423 15. Tenor JL, Oehlers SH, Yang JL, Tobin DM, Perfect JR. 2015. Live imaging of host-parasite interactions in a zebrafish
424 infection model reveals cryptococcal determinants of virulence and central nervous system invasion. mBio
425 6:e01425-15.

426 16. Srikanta D, Yang M, Williams M, Doering TL. 2011. A Sensitive High-Throughput Assay for Evaluating Host-Pathogen
427 Interactions in *Cryptococcus neoformans* Infection. PLOS ONE 6:e22773.

428 17. Chun CD, Madhani HD. 2010. Ctr2 links copper homeostasis to polysaccharide capsule formation and phagocytosis
429 inhibition in the human fungal pathogen *Cryptococcus neoformans*. PLOS ONE 5:e12503.

430 18. Srikanta D, Hole CR, Williams M, Khader SA, Doering TL. 2017. RNA interference screening reveals host CaMK4 as a
431 regulator of cryptococcal uptake and pathogenesis. Infect Immun 85:e00195-17.

432 19. Liu OW, Chun CD, Chow ED, Chen C, Madhani HD, Noble SM. 2008. Systematic genetic analysis of virulence in the
433 human fungal pathogen *Cryptococcus neoformans*. Cell 135:174–188.

434 20. Kaur G, Dufour JM. 2012. Cell lines: Valuable tools or useless artifacts. Spermatogenesis 2:1–5.

435 21. Merly L, Smith SL. 2017. Murine RAW 264.7 cell line as an immune target: are we missing something? Im-
436 munopharmacol Immunotoxicol 39:55–58.

437 22. Pan C, Kumar C, Bohl S, Klingmueller U, Mann M. 2009. Comparative proteomic phenotyping of cell lines and pri-
438 mary cells to assess preservation of cell type-specific functions. Mol Cell Proteomics MCP 8:443–450.

439 23. Chang AL, Hole CR, Doering TL. 2019. An automated assay to measure phagocytosis of *Cryptococcus neoformans*.
440 Curr Protoc Microbiol 53:e79.

441 24. Yoneda A, Doering TL. 2006. A Eukaryotic Capsular Polysaccharide Is Synthesized Intracellularly and Secreted via
442 Exocytosis. Mol Biol Cell 17:5131–5140.

443 25. Baba T, Balla T. 2020. Emerging roles of phosphatidylinositol 4-phosphate and phosphatidylinositol 4,5-bisphos-
444 phate as regulators of multiple steps in autophagy. J Biochem (Tokyo) 168:329–336.

445 26. Di Paolo G, De Camilli P. 2006. Phosphoinositides in cell regulation and membrane dynamics. Nature. Nature Pub-
446 lishing Group.

447 27. Santiago-Tirado FH, Bretscher A. 2011. Membrane-trafficking sorting hubs: cooperation between PI4P and small
448 GTPases at the trans-Golgi network. Trends Cell Biol 21:515–525.

449 28. Del Bel LM, Brill JA. 2018. Sac1, a lipid phosphatase at the interface of vesicular and nonvesicular transport. Traffic
450 19:301–318.

451 29. Agustinho DP, Miller LC, Li LX, Doering TL. 2018. Peeling the onion: The outer layers of *Cryptococcus neoformans*.
452 Mem Inst Oswaldo Cruz 113:1–8.

453 30. Reuwsaat JCV, Agustinho DP, Motta H, Chang AL, Brown H, Brent MR, Kmetzsch L, Doering TL. 2021. The transcrip-
454 tion factor Pdr802 regulates titan cell formation and pathogenicity of *Cryptococcus neoformans*. mBio 12:e03457-
455 20.

456 31. Hughes WE, Cooke FT, Parker PJ. 2000. Sac phosphatase domain proteins. Biochem J 350:337–352.

457 32. Kearns BG, McGee TP, Mayinger P, Gedvilaite A, Phillips SE, Kagiwada S, Bankaitis VA. 1997. Essential role for diacyl-
458 glycerol in protein transport from the yeast Golgi complex. Nature 387:101–105.

459 33. Del Bel LM, Griffiths N, Wilk R, Wei H-C, Blagoveshchenskaya A, Burgess J, Polevoy G, Price JV, Mayinger P, Brill JA.
460 2018. The phosphoinositide phosphatase Sac1 regulates cell shape and microtubule stability in the developing *Dro-*
461 *sophila* eye. Dev Camb Engl 145:dev151571.

462 34. Chang YC, Kwon-Chung KJ. 1994. Complementation of a capsule-deficient mutation of *Cryptococcus neoformans*
463 restores its virulence. Mol Cell Biol 14:4912–4919.

464 35. Chang YC, Penoyer LA, Kwon-Chung KJ. 1996. The second capsule gene of *Cryptococcus neoformans*, CAP64, is es-
465 sential for virulence. Infect Immun 64:1977–1983.

466 36. Chang YC, Kwon-Chung KJ. 1998. Isolation of the third capsule-associated gene, *CAP60*, required for virulence in
467 *Cryptococcus neoformans*. Infect Immun 66:2230–2236.

468 37. Chang YC, Kwon-Chung KJ. 1999. Isolation, characterization, and localization of a capsule-associated gene, *CAP10*,
469 of *Cryptococcus neoformans*. J Bacteriol 181:5636–5643.

470 38. Chun CD, Brown JCS, Madhani HD. 2011. A major role for capsule-independent phagocytosis-inhibitory mecha-
471 nisms in mammalian infection by *Cryptococcus neoformans*. Cell Host Microbe 9:243–251.

472 39. Bojarczuk A, Miller KA, Hotham R, Lewis A, Ogryzko NV, Kamuyango AA, Frost H, Gibson RH, Stillman E, May RC,
473 Renshaw SA, Johnston SA. 2016. *Cryptococcus neoformans* intracellular proliferation and capsule size determines
474 early macrophage control of infection. Sci Rep 6:1–15.

475 40. Reuwsaat JCV, Doering TL, Kmetzsch L. 2021. Too much of a good thing: Overproduction of virulence factors impairs
476 cryptococcal pathogenicity. Microb Cell 8:108–110.

477 41. Levine TP, Munro S. 2002. Targeting of Golgi-specific pleckstrin homology domains involves both PtdIns 4-kinase-
478 dependent and -independent components. Curr Biol CB 12:695–704.

479 42. Horianopoulos LC, Lee CWJ, Hu G, Caza M, Kronstad JW. 2021. Dnj1 promotes virulence in *Cryptococcus neofor-*
480 *mans* by maintaining robust endoplasmic reticulum homeostasis under temperature stress. Front Microbiol 12.

481 43. Wang ZA, Griffith CL, Skowyra ML, Salinas N, Williams M, Maier EJ, Gish SR, Liu H, Brent MR, Doering TL. 2014.
482 *Cryptococcus neoformans* dual GDP-mannose transporters and their role in biology and virulence. Eukaryot Cell
483 13:832–842.

484 44. Johansen J, Ramanathan V, Beh CT. 2012. Vesicle trafficking from a lipid perspective. Cell Logist 2:151–160.

485 45. Ling Y, Hayano S, Novick P. 2014. Osh4p is needed to reduce the level of phosphatidylinositol-4-phosphate on secre-
486 tory vesicles as they mature. Mol Biol Cell 25:3389–3400.

487 46. Fei W, Shui G, Zhang Y, Krahmer N, Ferguson C, Kapterian TS, Lin RC, Dawes IW, Brown AJ, Li P, Huang X, Parton RG,
488 Wenk MR, Walther TC, Yang H. 2011. A role for phosphatidic acid in the formation of “supersized” lipid droplets.
489 PLoS Genet 7.

490 47. Choy HL, Gaylord EA, Doering TL. 2023. Ergosterol distribution controls surface structure formation and fungal
491 pathogenicity. mBio 14:e01353-23.

492 48. Klutts JS, Doering TL. 2008. Cryptococcal xylosyltransferase 1 (Cxt1p) from *Cryptococcus neoformans* plays a direct
493 role in the synthesis of capsule polysaccharides. J Biol Chem 283:14327–14334.

494 49. Basenko EY, Pulman JA, Shanmugasundram A, Harb OS, Crouch K, Starns D, Warrenfeltz S, Aurrecoechea C, Chris-
495 tian J. Stoeckert J, Kissinger JC, Roos DS, Hertz-Fowler C. 2018. FungiDB: an integrated bioinformatic resource for
496 fungi and oomycetes. J Fungi 4.

497 50. Boodwa-Ko D, Doering TL. 2024. A quick reCAP: Discovering *Cryptococcus neoformans* capsule mutants. J Fungi Ba-
498 sel Switz 10:114.

499 51. Arras SDM, Chitty JL, Blake KL, Schulz BL, Fraser JA. 2015. A genomic safe haven for mutant complementation in
500 *Cryptococcus neoformans*. PLoS ONE 10:e0122916.

501 52. Jin J-H, Lee K-T, Hong J, Lee D, Jang E-H, Kim J-Y, Lee Y, Lee S-H, So Y-S, Jung K-W, Lee D-G, Jeong E, Lee M, Jang Y-B,
502 Choi Y, Lee MH, Kim J-S, Yu S-R, Choi J-T, La J-W, Choi H, Kim S-W, Seo KJ, Lee Y, Thak EJ, Choi J, Averette AF, Lee Y-H,
503 Heitman J, Kang HA, Cheong E, Bahn Y-S. 2020. Genome-wide functional analysis of phosphatases in the pathogenic
504 fungus *Cryptococcus neoformans*. 1. Nat Commun 11:4212.

505 53. Nielsen K, Cox GM, Wang P, Toffaletti DL, Perfect JR, Heitman J. 2003. Sexual cycle of *Cryptococcus neoformans* var.
506 *grubii* and virulence of congenic a and α isolates. Infect Immun 71:4831–4841.

507 54. Fernandes KE, Fraser JA, Carter DA. 2022. Lineages derived from *Cryptococcus neoformans* type strain H99 support
508 a link between the capacity to be pleomorphic and virulence. mBio 13:e00283-22.

509 55. Godi A, Campli AD, Konstantakopoulos A, Tullio GD, Alessi DR, Kular GS, Daniele T, Marra P, Lucocq JM, Matteis
510 MAD. 2004. FAPPs control Golgi-to-cell-surface membrane traffic by binding to ARF and PtdIns(4)P. 5. Nat Cell Biol
511 6:393–404.

512 56. Dowler S, Currie RA, Campbell DG, Deak M, Kular G, Downes CP, Alessi DR. 2000. Identification of pleckstrin-homol-
513 ogy-domain-containing proteins with novel phosphoinositide-binding specificities. Biochem J 351:19–31.

514 57. Walther TC, Chung J, Farese RV. 2017. Lipid droplet biogenesis. Annu Rev Cell Dev Biol 33:491–510.

515 58. Fei W, Shui G, Gaeta B, Du X, Kuerschner L, Li P, Brown AJ, Wenk MR, Parton RG, Yang H. 2008. Fld1p, a functional
516 homologue of human seipin, regulates the size of lipid droplets in yeast. J Cell Biol 180:473–482.

517 59. Breuer MR, Dasgupta A, Vasselli JG, Lin X, Shaw BD, Sachs MS. 2022. The antidepressant sertraline induces the for-
518 mation of supersized lipid droplets in the human pathogen *Cryptococcus neoformans*. J Fungi 8:642.

519 60. Solanko KA, Modzel M, Solanko LM, Wüstner D. 2016. Fluorescent sterols and cholesteryl esters as probes for intra-
520 cellular cholesterol transport. Lipid Insights 8:95–114.

521 61. Menon AK. 2018. Sterol gradients in cells. Curr Opin Cell Biol 53:37–43.

522 62. von Filseck JM, Vanni S, Mesmin B, Antonny B, Drin G. 2015. A phosphatidylinositol-4-phosphate powered ex-
523 change mechanism to create a lipid gradient between membranes. 1. Nat Commun 6:6671.

524 63. Santiago-Tirado FH, Legesse-Miller A, Schott D, Bretscher A. 2011. Phosphatidylinositol 4-phosphate and Rab inputs
525 collaborate in myosin-V-dependent transport of secretory compartments in yeast. Dev Cell 20:47–59.

526 64. Bankaitis VA, Garcia-Mata R, Mousley CJ. 2012. Golgi membrane dynamics viewed through a lens of lipids. Curr Biol
527 CB 22:R414–R424.

528 65. McFadden DC, Fries BC, Wang F, Casadevall A. 2007. Capsule structural heterogeneity and antigenic variation in
529 *Cryptococcus neoformans*. Eukaryot Cell 6:1464–1473.

530 66. Doering TL. 2009. How sweet it is! Cell wall biogenesis and polysaccharide capsule formation in *Cryptococcus*
531 *neoformans*. Annu Rev Microbiol 63:223–247.

532 67. Fu J, Hettler E, Wickes BL. 2006. Split marker transformation increases homologous integration frequency in *Crypto-*
533 *coccus neoformans*. Fungal Genet Biol 43:200–212.

534 68. Huang MY, Joshi MB, Boucher MJ, Lee S, Loza LC, Gaylord EA, Doering TL, Madhani HD. 2022. Short homology-di-
535 rected repair using optimized Cas9 in the pathogen *Cryptococcus neoformans* enables rapid gene deletion and tag-
536 ging. Genetics 220:iyab180.

537 69. Upadhya R, Lam WC, Maybruck B, Donlin MJ, Chang AL, Kayode S, Ormerod KL, Fraser JA, Doering TL, Lodge JK.
538 2017. A fluorogenic *C. neoformans* reporter strain with a robust expression of m-cherry expressed from a safe ha-
539 ven site in the genome. Fungal Genet Biol FG B 108:13–25.

540 70. Chang AL, Kang Y, Doering TL. 2019. Cdk8 and Ssn801 regulate oxidative stress resistance and virulence in *Crypto-*
541 *coccus neoformans*. mBio 10:e02818-18.

542 71. Cherniak R, Morris LC, Anderson BC, Meyer SA. 1991. Facilitated isolation, purification, and analysis of glucuronoxy-
543 lomannan of *Cryptococcus neoformans*. Infect Immun 59:59–64.

544 72. Willis LM, Stupak J, Richards MR, Lowary TL, Li J, Whitfield C. 2013. Conserved glycolipid termini in capsular poly-
545 saccharides synthesized by ATP-binding cassette transporter-dependent pathways in Gram-negative pathogens.
546 Proc Natl Acad Sci 110:7868–7873.

547 73. Ashburner M, Ball CA, Blake JA, Botstein D, Butler H, Cherry JM, Davis AP, Dolinski K, Dwight SS, Eppig JT, Harris MA,
548 Hill DP, Issel-Tarver L, Kasarskis A, Lewis S, Matese JC, Richardson JE, Ringwald M, Rubin GM, Sherlock G. 2000.
549 Gene Ontology: tool for the unification of biology. 1. Nat Genet 25:25–29.

550 74. The Gene Ontology Consortium, Aleksander SA, Balhoff J, Carbon S, Cherry JM, Drabkin HJ, Ebert D, Feuermann M,
551 Gaudet P, Harris NL, Hill DP, Lee R, Mi H, Moxon S, Mungall CJ, Muruganugan A, Mushayahama T, Sternberg PW,
552 Thomas PD, Van Auken K, Ramsey J, Siegele DA, Chisholm RL, Fey P, Aspromonte MC, Nugnes MV, Quaglia F, Tosatto
553 S, Giglio M, Nadendla S, Antonazzo G, Attrill H, dos Santos G, Marygold S, Strelets V, Tabone CJ, Thurmond J, Zhou P,
554 Ahmed SH, Asanitthong P, Luna Buitrago D, Erdol MN, Gage MC, Ali Kadhum M, Li KYC, Long M, Michalak A, Pesala
555 A, Pritazahra A, Saverimuttu SCC, Su R, Thurlow KE, Lovering RC, Logie C, Oliferenko S, Blake J, Christie K, Corbani L,
556 Dolan ME, Drabkin HJ, Hill DP, Ni L, Sitnikov D, Smith C, Cuzick A, Seager J, Cooper L, Elser J, Jaiswal P, Gupta P,
557 Jaiswal P, Naithani S, Lera-Ramirez M, Rutherford K, Wood V, De Pons JL, Dwinell MR, Hayman GT, Kaldunski ML,
558 Kwitek AE, Laulederkind SJF, Tutaj MA, Vedi M, Wang S-J, D'Eustachio P, Aimo L, Axelsen K, Bridge A, Hyka-Nouspikel
559 N, Morgat A, Aleksander SA, Cherry JM, Engel SR, Karra K, Miyasato SR, Nash RS, Skrzypek MS, Weng S, Wong ED,
560 Bakker E, Berardini TZ, Reiser L, Auchincloss A, Axelsen K, Argoud-Puy G, Blatter M-C, Boutet E, Breuza L, Bridge A,
561 Casals-Casas C, Coudert E, Estreicher A, Livia Famiglietti M, Feuermann M, Gos A, Gruaz-Gumowski N, Hulo C, Hyka-
562 Nouspikel N, Jungo F, Le Mercier P, Lieberherr D, Masson P, Morgat A, Pedruzzi I, Pourcel L, Poux S, Rivoire C,
563 Sundaram S, Bateman A, Bowler-Barnett E, Bye-A-Jee H, Denny P, Ignatchenko A, Ishtiaq R, Lock A, Lussi Y, Magrane
564 M, Martin MJ, Orchard S, Raposo P, Speretta E, Tyagi N, Warner K, Zaru R, Diehl AD, Lee R, Chan J, Diamantakis S,

565 Raciti D, Zarowiecki M, Fisher M, James-Zorn C, Ponferrada V, Zorn A, Ramachandran S, Ruzicka L, Westerfield M.
566 2023. The Gene Ontology knowledgebase in 2023. Genetics 224:iyad031.

567 75. Thompson JD, Higgins DG, Gibson TJ. 1994. CLUSTAL W: improving the sensitivity of progressive multiple sequence
568 alignment through sequence weighting, position-specific gap penalties and weight matrix choice. Nucleic Acids Res
569 22:4673–4680.

570

571 **FIGURE LEGENDS**

572 **Figure 1.** Screen results. (A) Schematic of screening workflow. Asterisk indicates *SAC1* in the diagram at right. (B and C)
573 Uptake scores (as defined in the text) for the 93 mutants identified as hits when screened against both (B) BMDM and (C)
574 HMDM. The value under each bar represents the center of the bin and 1.0 is the WT value. (D) Selected GO terms that are
575 enriched in the 93 dual hits from the uptake screen. X-axis, number of hit gene IDs which fall within each category. (E)
576 Capsule score (capsule thickness relative to that of WT under inducing conditions) for 131 mutants identified as hits in the
577 capsule screen, plotted as in (B) and (C). (F) Selected GO terms that are enriched in hits from the capsule screen, plotted
578 as in (D). For panels D and F, bold text denotes categories uniquely enriched for each screen; note that not all categories
579 are listed.

580

581 **Figure 2.** Cells lacking active Sac1 show increased uptake by phagocytes and smaller capsules. (A) Uptake and capsule
582 screen results for cells lacking CKF44_06080. (B) Alignment of *C. neoformans* and *S. cerevisiae* sequences that include
583 the Sac1 catalytic motif. Blue, identical residues; asterisk, residue mutated to alanine in the $SAC1^{D456A}$ strain. (C) India ink
584 negative stain of the indicated strains grown for 24 hours in DMEM at 37°C with 5% CO_2. Capsule thickness in µm (mean ±
585 SD) is noted below each panel. All primary images are at the same magnification; scale bar, 10 µm. For this and other
586 microscopy figures, any region demarcated by a small square is enlarged in the inset at upper right. (D) Distribution of
587 normalized capsule thicknesses for the indicated strains. At least 96 cells were measured for each strain as described in
588 the Methods. *, $p<0.0332$; ****, $p<0.0001$ by 2-way ANOVA with Tukey's multiple comparison test; ns, not significant.

589

590 **Figure 3**. Sac1 is important for virulence in a mouse infection model. (A) Lung and (B) burden of C57BL/6 mice (groups of
591 8-10) sacrificed 14 days after intranasal infection with $5x10^4$ fungal cells (upper dotted line). Plots show median (bold black
592 line) with interquartile range. Lower dotted line, limit of detection. Each symbol represents one mouse. ****, p<0.0001;
593 comparison with no stars shown are not significant. Significance was calculated using 2-way ANOVA with Tukey's multiple
594 comparison test.
595
596 **Figure 4.** Sac1 regulates substrate distribution and stress sensitivity. (A) FAPP1-mNeonGreen (mNG) localization in cells
597 grown in YPD at 30°C. All primary images are at the same magnification; scale bar, 10 µm. (B) Serial 10-fold dilutions of the
598 indicated strains plated on YPD alone or containing 0.01% SDS (SDS), 0.05% Congo Red (CR), or 2 µg/mL Amphotericin B
599 (AMB), incubated at 30 and 37°C. *inact* = $SAC1^{D456A}$.
600
601 **Figure 5.** Sac1 is essential for proper lipid trafficking in host-like conditions. (A) Transmission electron micrographs of cells
602 grown in the indicated medium. White asterisks, example lipid droplet structures, likely distorted during sample prep; scale
603 bar, 1 µm. (B) Nile Red stain of the indicated strains with (C) quantification of the observed staining pattern. (D) Filipin
604 staining of cells grown in DMEM. YPD grown cells in Panel A were grown overnight at 30 °C, all other cells were grown for
605 24 h in DMEM at 37°C with 5% CO_2. Scale bar, 10 µm. All images within each experiment are shown at the same magnifi-
606 cation.
607
608 **Figure 6.** Supplementation with exogenous fatty acid partially restores *sac1*Δ growth and morphology but not capsule
609 biosynthesis. (A) Serial 10-fold dilutions of WT and *sac1*Δ cells grown for 24 hours (at 37°C with 5% CO_2) in DMEM supple-
610 mented with BSA alone (-), or with 8, 40, or 200 µM myristic acid conjugated to BSA (increasing amounts indicated by the
611 triangle). (B) India ink negative stain of WT and *sac1*Δ cells grown in DMEM at 37°C with 5% CO_2, supplemented as indicated
612 with BSA alone or 200 µM myristic acid conjugated to BSA. Capsule thickness in µm (mean ± SD) is noted below each panel.
613 All primary images are to the same magnification; scale bar, 10 µm.
614
615 **Figure 7.** Sac1 controls the secretory pathway to modulate capsule size and composition. (A) Secreted acid phosphatase
616 activity, normalized to cell number, over time after a shift to phosphate-depleted medium. (B) Confocal imaging of Cxt1-

617 mNG in the indicated strain backgrounds with (C) quantification of observed staining patterns. Punctate: 3 or more

618 puncta present; Intermediate: puncta and diffuse signal; Diffuse/low: diffuse signal or <3 puncta. Images are to the same

619 scale; scale bar, 10 µm. (D) Shed GXM quantified by ELISA. For both (A) and (D), mean ± SD for one representative experi-

620 ment of three biological replicate studies is shown. (E) Left, GXM composition; right, subunit structure of GXM.

621 **SUPPLEMENTAL MATERIAL FOR GAYLORD ET AL**

622

623 **Supplemental Methods**

624 BMDM preparation

625 BMDMs were isolated as in (70) from 9-week old C57BL/6J mice and frozen in 90% FBS, 10% DMSO at 10^7 cells/mL.
626 Thawed cells were differentiated for 9 days in RPMI-1640 with L-glutamine (Sigma) with 30% L-cell supernatant and 20%
627 heat-inactivated fetal bovine serum (Gibco), with regular media changes. BMDM were resuspended in 10 mL ice cold PBS
628 and isolated using 2.5 µg anti-mouse F4/80 biotin (clone BM8, eBiosciences) plus 0.5 µg mouse BD FC-Block (BD
629 Pharmingen) with anti-biotin microbeads (Miltenyi Biotec) and a MACS separation column (Miltenyi Biotec).

630 Human macrophage preparation

631 Leukoreduction system (LRS) chambers were obtained from anonymous donors and human peripheral blood mon-
632 onuclear cells (PMBC) were isolated by Ficoll-Paque centrifugation (Lymphoprep; Axis-Shield). $5x10^7$ PMBC were allowed
633 to adhere to a treated culture dish (Corning) for 2 hours at 37°C with 5% CO_2. Detached cells were removed, and adherent
634 cells were maintained in RPMI-1640 differentiation media containing L-glutamine (Sigma), 10% fetal bovine serum (Sigma),
635 1% penicillin streptomycin (Fisher), 1% sodium pyruvate (Corning), 50ng/mL human recombinant M-CSF (Fisher), and 1%
636 MEM non-essential amino acids (Corning). Medium was replaced every two days and adherent cells were harvested on
637 day 6 using Cell Stripper (Corning).

638 Uptake screen

639 Assays were performed using a modification of our prior method (23). Host cells were seeded in flat clear bottom
640 black polystyrene TC-treated 96-well plates (Corning) at a density of 10^5 cells/well and incubated for one day at 37°C with
641 5% CO_2. *C. neoformans* strains were cultured from frozen stocks in glycerol/Yeast Extract-Peptone-Dextrose medium (YPD)
642 in 96 well format for 18-24 h at 30°C with shaking (800 rpm) (Southwest Science, SBT1500-H). At least 2 µL of cells were
643 then sub-cultured in 100 µL YPD and grown for 18-24 h as above. After sub-culture, cells were sedimented (3000 g, 2 min,
644 RT), washed twice with 200 µL of PBS, washed once with 200 µL McIlvaine's Buffer [pH 6], and resuspended in 80 µL of the
645 same. Cells were then stained with 5 mg/mL Lucifer Yellow (30 min, RT, 650 rpm) and resuspended in 100 µL of PBS. To
646 account for variation in growth rates of *C. neoformans* mutants, OD_{600} was used to roughly standardize cell number and
647 maintain results in the linear range of the assay. To do this, individual mutants were categorized as having high, medium,

648 or low growth based on the OD_{600} after resuspension in PBS and the average value of each group was used to prepare wells
649 with approximately 10^7 fungal cells/mL in PBS. Fungal cells were then opsonized with 10% by volume C57Bl6/J mouse
650 serum (for BMDM) or human serum from male AB plasma (for HMDM, Sigma) for 30 minutes at 37°C at 250 rpm. Opso-
651 nized cells were then added to wells containing RPMI and macrophages at a multiplicity of infection of 20 (BMDM) or 30
652 (HMDM). Cells were co-incubated for one hour at 37°C with 5% CO_2 to allow uptake and washed. This and the following
653 washes were performed using a Biotek ELx405 Microplate Washer (2 washes, PBS). Adherent fungal cells were stained
654 with 150 µL of 5 µg/mL Calcofluor White (Sigma) (15 min, 4°C, static). Samples were then washed, fixed with 4% formal-
655 dehyde (10 min, RT), washed, permeabilized with 1 mg/mL saponin (20 min, RT), washed, and stained with 50 µg/mL
656 propidium iodide (15 min, RT). Imaging was performed on a BioTek Cytation 3 imager collecting 12 images per well in a
657 4x3 grid pattern.

658 A separate plate of each *C. neoformans* strain alone was counted to allow normalization for the number of cells of
659 each mutant strain that were used in the assay. The phagocytic index for each mutant was determined by calculating the
660 number of internalized cells per macrophage and normalizing this to the value for WT KN99 and the number of fungi
661 added. An uptake score was then calculated for each well as fold-change of the normalized phagocytic index compared
662 either to the plate median (for the initial screen of Madhani library plates) or to WT (for the follow-up screens with BMDM
663 and HMDM). For the initial screen of the Madhani deletion collection, we calculated the first quartile (Q1), third quartile
664 (Q3), and interquartile range (IQR) for each plate. We defined hits as those below Q1-c*IQR or above Q3-c*IQR, where c
665 was calculated using a targeted error rate, α, of 0.01. For the second round of screening in BMDM and HMDM, we used
666 an internal WT control and defined hits as those strains whose uptake scores differed from WT in a statistically significant
667 way, using Dunnett's 1-way ANOVA and a p value cutoff of 0.05.

668 Capsule screen

669 Strains identified as hits in the uptake assay and wild type control cells were cultured in YPD from frozen stocks in
670 glycerol/YPD in 96 well format (ON, 30 °C, 800 rpm); 10 µL aliquots were then sub-cultured into 190 µL fresh YPD and
671 grown for an additional 24 h. Cells were then sedimented (3000 g, RT) and resuspended in 200 µL DMEM. To achieve the
672 low cell density necessary for optimum capsule induction, the average OD_{600} of the plate was used to calculate the volume
673 of cells to resuspend in 150 µL DMEM to achieve an average OD_{600} of 0.01. Capsule induction was performed in a 96-well
674 glass-bottom plate coated with poly-lysine (Eppendorf) and incubated for 24 h at 37°C with 5% CO_2. KN99α cells grown

675 overnight in YPD were added to empty wells 10 min before the induction ended to serve as an uninduced control. Follow-
676 ing induction, cells were stained and imaged as published previously (30). Briefly, the capsules were stained with anti-
677 capsular monoclonal antibody 302 conjugated to Alexa Fluor 488 (Molecular Probes) and the cell walls stained with Calco-
678 fluor White (MP Biomedicals). Imaging was performed on a BioTek Cytation 3 imager collecting 64 images per well in an
679 8x8 grid pattern. Images were prepared, annotated, and cell wall and capsule diameters for annotated cells calculated as
680 described previously (30). Capsule thickness was defined as the difference between cell wall and capsule diameters. A
681 negative control value (mean capsule thickness of WT cells grown in YPD in the same plate) was subtracted and the result
682 normalized to the value for similarly-corrected positive control samples (WT cells induced in the same plate) to yield a
683 capsule score. Hypocapsular and hypercapsular hits were categorized as those with capsule scores of less than 0.5 or more
684 than 2.0, respectively.

685 Gene ontology enrichment analysis

686 Gene ontology (GO) analysis was performed using FungiDB, using both manually curated and computationally
687 predicted GO terms (49, 73, 74). GO categories that were enriched with a P-value cutoff of 0.01 were manually selected
688 for each screen to minimize over-representation of redundant phenotypes.

689 Strain construction and validation

690 *sac1Δ*, *SAC1* complement, and *SAC1*^{D456A} strains were engineered using biolistic transformation with a split-marker
691 strategy (67) in a KN99α background. Design of the catalytically-inactivated construct was based on alignment (75) to the
692 *S. cerevisiae* S288C Sac1 amino acid sequence. mNeonGreen-tagged strains were generated using pBHM2404, a gift from
693 Hiten Madhani (Addgene 173441). PI4P-binding constructs were generated using pRS406-PHO5-GFP-hFAPP1 PH domain,
694 a gift from Tim Levine (Addgene 58723) (41). This sequence was placed between a *TEF1* promoter and terminator and
695 inserted into the Safe Haven 2 (SH2) region of the genome (69). All fluorescent constructs were generated using CRISPR
696 with short homology-directed repair (68). Transformants were confirmed by appropriate antifungal resistance, PCR, and
697 whole genome sequencing.

698 To test complementation of *sac1*Δ by the corresponding *S. cerevisiae* sequence, the *SAC1* gene was amplified from
699 *S. cerevisiae* strain S288C and inserted into plasmid pMSC042-neo between an *ACT1* promoter and *TRP1* terminator. This
700 construct (containing the promoter, *SAC1* sequence, terminator and antifungal resistance marker) was inserted into the
701 SH2 region of WT and *sac1*Δ cells using CRISPR (68, 69). Total RNA was extracted from cells grown in YPD and DMEM using

702 TRIzol Reagent (Thermo Fisher) and cDNA was synthesized using the SuperScript III First-Strand Synthesis SuperMix kit
703 (Thermo Fisher). PCR amplification of an S288C Sac1-specific sequence from the cDNA confirmed expression of the S288C
704 *SAC1* gene in both backgrounds (Fig. S1B).

705 Fungal cell growth and capsule induction

706 *C. neoformans* strains were grown from glycerol stocks on YPD plates for 2 days at 30°C. Overnight cultures were
707 inoculated from single colonies into 4 mL of YPD medium and grown overnight at 30°C with shaking (unless otherwise
708 noted). For all capsule induction experiments, overnight cultures were washed in sterile PBS, inoculated into DMEM at
709 10^6 cells/mL, and grown statically at 37°C with 5% CO_2 for 16-24 hours (as indicated in the text).

710 Virulence studies

711 All animal protocols were approved by the Washington University Institutional Animal Care and Use Committee
712 (Protocol #20-0108) and care was taken to minimize animal handling and discomfort. 6-8-week old female C57BL/6 mice
713 (The Jackson Laboratory) were anesthetized by subcutaneous injection of 1.20 mg ketamine and 0.24 mg xylazine in 110
714 µL sterile PBS. For 14-day infections, mice were intranasally infected with 5×10^4 cryptococcal cells. For time course infec-
715 tion, mice were infected with 1.25×10^4 cryptococcal cells and sacrificed at 6-, 12-, and 18-days post infection. For both
716 infections, the lungs and brains were harvested, homogenized, and plated on YPD agar for calculation of fungal organ
717 burden.

718 Stress plate dot spotting

719 Overnight cultures were pelleted and washed twice in PBS, then diluted to 10^7 cells/mL. 4 µL of this stock and four
720 serial 1:10 dilutions were spotted onto YPD agar and incubated at both 30 and 37°C for 48 hours. To impose plasma
721 membrane stress, the YPD was supplemented with 0.01% sodium dodecyl sulfate or 1 µg/ml amphotericin B; to impose
722 cell wall stress, the YPD was supplemented with 0.05% Congo red.

723 Acid phosphatase secretion assay

724 Single colonies were inoculated into 5 mL YPD, grown shaking at 30°C for 6 h, sub-cultured into 25 mL MM-KH_2PO_4
725 (0.5% KH_2PO_4, 15 mM glucose, 10 mM $MgSO_4 \cdot 7H_2O$, 13 mM glycine, 3.0 µM thiamine), and grown overnight at 30°C. Cells
726 were then pelleted, washed twice with MM-KCl (0.5% KCl, 15 mM glucose, 10 mM $MgSO_4 \cdot 7H_2O$, 13 mM glycine, 3.0 µM
727 thiamine), and resuspended in 50 mL MM-KCl at 10^7 cells/mL. Cultures were grown at 30°C with shaking, and 2 mL aliquots
728 were collected at each timepoint. For each, pelleted cells were resuspended in 400 µL substrate buffer (2.5 mM para-

729 nitrophenylphosphate in 50 mM acetate buffer, pH 4.0, Sigma 71768-5G), incubated at 37°C for 5 minutes, and the reac-
730 tion stopped with 800 µL saturated Na_2CO_3. Acid phosphatase secretion was quantified using absorbance at 420 nm, cor-
731 rected by subtraction of a cell-free blank value, and normalized to cell density using OD_{600}.

732 GXM ELISA

733 Cultures were induced in DMEM for the indicated times, at which point cells were removed by centrifugation
734 (3000 x g, 5 min, RT), the supernatant fraction filtered through a 0.2µm filter, and the filtrate diluted 1:500 in PBS. Flat-
735 bottom Immulon 1B microtiter plates (Thermo Scientific) were coated overnight with a 1 µg/ml mix of anti-GXM antibodies
736 339 and F12D2γ in PBS. This and the following incubations were performed at room temperature. The plates were washed
737 twice with 200 µL PBS with 0.5% TWEEN 20 (PBST), blocked for 90 min with 200 µL 1% BSA in PBST. The blocking buffer
738 was replaced with 100 µL PBST and 100 µL of filtered sample was added and incubated for 90 min. The plate was then
739 washed three times as above and the bound GXM was probed with HRP-labeled mAb 339/F12D2γ, incubated for 1 minute
740 with KPL TMB Microwell Peroxidase Substrate (SeraCare), developed, and quantified using absorbance at 450 nm.

741 Imaging

742 For fluorescence and confocal microscopy, cells were grown as indicated above and washed twice in PBS. For
743 capsule visualization, cells were resuspended in India ink in PBS (1:2, v:v) and imaged on a ZEISS Axio Imager M2 fluores-
744 cence microscope. Capsule thickness was measured manually in ImageJ, using a total of at least 96 cells from at least six
745 randomly-chosen fields of view. To stain neutral lipids, a 0.01% Nile Red stock in acetone was diluted to a working con-
746 centration of 0.0005% in PBS. Cells were incubated in 1 mL working Nile Red solution for 15 min in the dark, rotating. Cells
747 were washed twice in PBS, resuspended in PBS, and imaged as above. For quantification of morphology, a minimum of 60
748 cells from randomly-chosen slide coordinates were examined. For filipin staining, cells were incubated in a freshly pre-
749 pared solution of 5 µg/mL filipin (Millipore Sigma, F9765-25MG) in DMSO for 15 minutes at room temperature, rotating,
750 then washed twice with PBS before imaging as above. To visualize FAPP1-mNeonGreen and Cxt1- mNeonGreen, cells were
751 imaged using a Zeiss LSM880 confocal microscope. For quantification of morphology, a minimum of 94 cells from ran-
752 domly-chosen slide coordinates were examined. For electron microscopy, cells were grown overnight in YPD or induced
753 for 24 hours in DMEM before processing as in (47), except that the first incubation in 0.1 M sodium cacodylate buffer was
754 performed for 2 h at RT.

755 Lipid supplementation

756 For lipid supplementation, a fatty acid stock solution (10 mM in ethanol) was diluted 1:10 into 4 mg/ml BSA in
757 DMEM and then sonicated (Bransonic 2 Ultrasonic Bath Sonicator) before addition to cultures as indicated. After 24-hour
758 of incubation (37°C, 5% CO_2), cells were serially diluted 1:10 and plated onto YPD agar, with the top spot representing the
759 undiluted culture.

760 GXM purification and analysis

761 GXM was isolated using selective precipitation of culture supernatants with hexadecyltrimethylammonium bro-
762 mide (CTAB) as described previously (48). Isolated material was hydrolyzed in trifluoroacetic acid for 3 hours at 100°C and
763 compositional analysis performed using high-performance anion-exchange chromatography with pulsed amperometric
764 detection on a Dionex ICS-6000 instrument (Thermo Scientific). Glycosyl linkage analysis was performed by the Complex
765 Carbohydrate Research Center at the University of Georgia using combined gas chromatography/mass spectrometry of
766 partially methylated alditol acetate derivatives following carboxyl reduction to detect uronic acids (modified from (72)).

767

768

769 **Supplemental Table Legends**

770

771 **Supplemental Table S1.** Uptake screen results. (S1A) All results from the initial BMDM uptake screen. (S1B) Hits from the
772 initial BMDM uptake screen. (S1C) All results from the second BMDM uptake screen. (S1D) Hits identified from the second
773 BMDM uptake screen. (S1E) All results from the HMDM uptake screen. (S1F) Hits from the HMDM uptake screen.

774

775 **Supplemental Table S2.** Capsule screen results. (S2A) All results from the capsule screen. (S2B) Hits identified from the
776 capsule screen. (S2C) Overlap hits identified in all three screens: HMDM, BMDM, and capsule.

777

778 **Supplemental Table S3.** Linkage analysis of WT, *sac1*Δ, and *SAC1* strains. Values are the percent area of relevant residue
779 peaks. Numbers in the header row refer to independently isolated samples.

780

781 **Supplemental Figure Legends**

782

783 **Supplemental Figure S1.** Overexpression of the *S. cerevisiae* Sac1 protein in *sac1*Δ does not restore *C. neoformans* capsule
784 synthesis. (A) Negative stain of the indicated strains grown for 24 hours in DMEM at 37°C with 5% CO_2, with the capsule
785 thickness in µm (mean ± SD). Scale bar, 10 µm. (B) Amplification of a unique 651 bp region of the S288C Sac1 coding
786 sequence from cDNA generated from fungal cells of the indicated strain grown in YPD shows that the *S. cerevisiae SAC1*
787 gene is expressed in both *C. neoformans* strains.

788

789 **Supplemental Figure S2.** Construction and validation of the $SAC1D^{456A}$ strain. (A) Strain construction strategy for *SAC1*
790 complement and SAC^{D456A} inactivated complement strains. (B) Normalized expression of *SAC1* in WT and $SAC1^{D456A}$ cells
791 grown for 24 hours in DMEM at 37°C with 5% CO_2. (C) Nucleotide sequence of $SAC1^{D456}$. Red, nucleotide differences from
792 WT *SAC1*.

793

794 **Supplemental Figure S3.** Cells lacking functional Sac1 have reduced virulence. (A) Lung and (B) brain burden of C57BL/6
795 mice sacrificed at the indicated days post infection (dpi) with 1.25×10^4 fungal cells of *ckf44_06080*Δ from the Madhani *C.*
796 *neoformans* deletion collection. Upper dotted line, inoculum. Lower dotted line, limit of detection. Each symbol represents
797 one mouse.
798
799 **Supplemental Figure S4.** PI4P content of WT and *sac1*Δ strains. Difference in median fluorescence intensity between
800 FAPP1-mNG expressing and control cells (ΔMFI) in WT and mutant backgrounds, grown in the indicated medium. ns, not
801 significant by unpaired t test.
802
803 **Supplemental Figure S5**. Dual staining with filipin and Nile Red. All cells were grown in DMEM for 24 hours at 37°C with
804 5% CO_2. DIC, Differential interference contrast. Scale bar, 10 µm.
805
806 **Supplemental Figure S6.** Supplementation with exogenous fatty acids partially restores growth of *sac1*Δ cells. Serial dilu-
807 tions of (left) WT or (right) *sac1*Δ cells grown for 24 hours in DMEM alone, DMEM supplemented with BSA, or DMEM with
808 100 µM of the indicated fatty acid sodium salt conjugated to 0.4 mg/mL BSA.

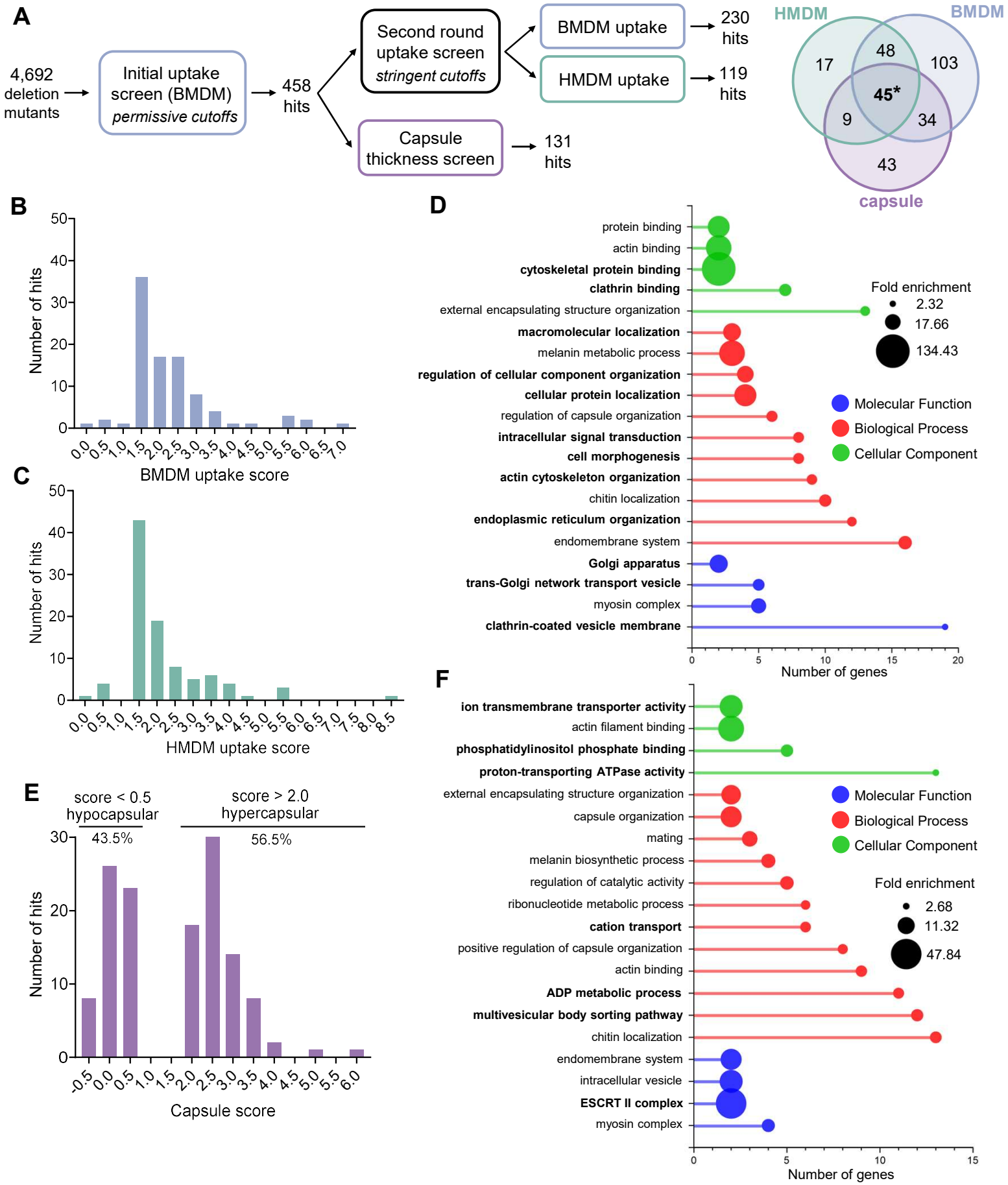

Figure 1. Screen results. (A) Left, schematic of screening workflow, and right, overlap of screen hits. Asterisk indicates *SAC1* in the diagram at right. **(B and C)** Uptake scores (as defined in the text) for the 93 mutants identified as hits when screened against both **(B)** BMDM and **(C)** HMDM. The value under each bar represents the center of the bin and 1.0 is the WT value. **(D)** Selected GO terms that are enriched in the 93 dual hits from the uptake screen. X-axis, number of hit gene IDs which fall within each category. **(E)** Capsule score (capsule thickness relative to that of WT under inducing conditions) for 131 mutants identified as hits in the capsule screen, plotted as in **(B)** and **(C)**. **(F)** Selected GO terms that are enriched in hits from the capsule screen, plotted as in **(D)**. For panels D and F, bold text denotes categories uniquely enriched for each screen; note that not all categories are listed.

A

Deleted gene	Annotation	Uptake score		Normalized capsule size
		BMDM	HMDM	
CKF44_06080	inositol/phosphatidylinositol phosphatase	2.25	1.83	0.39

B

Catalytic motif

*

Sc Sac1 V E I V N E Q H S V V R T N C M D C L D R T N V V Q S **(378-404)**

Cn Sac1 T Q V L T K Q T G V V R T N C M D C L D R T N V A Q A **(440-466)**

C

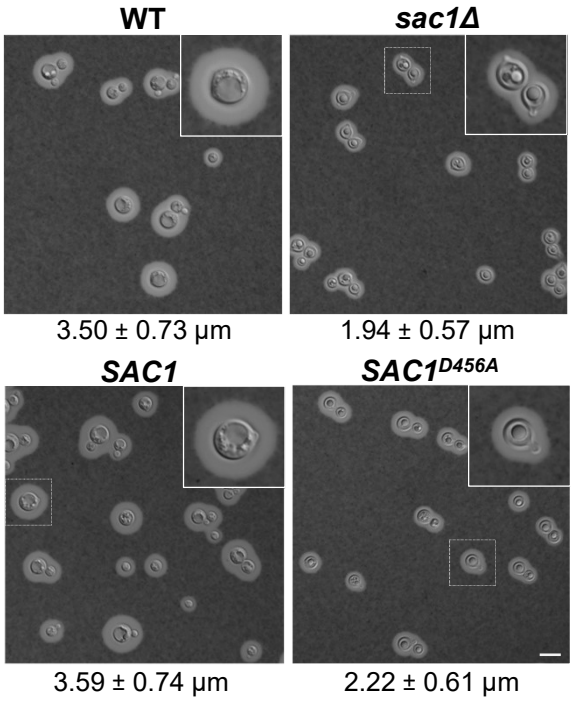

D

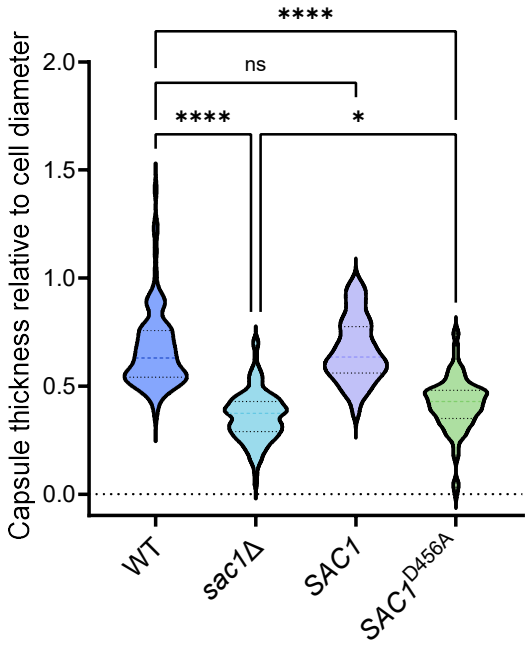

Figure 2. Cells lacking active Sac1 show increased uptake by phagocytes and smaller capsules. (A) Uptake and capsule screen results for cells lacking CKF44_06080. **(B)** Alignment of *C. neoformans* and *S. cerevisiae* sequences that include the Sac1 catalytic motif. Blue, identical residues; asterisk, residue mutated to alanine in the *SAC1*^{D456A} strain. **(C)** India ink negative stain of the indicated strains grown for 24 hours in DMEM at 37°C with 5% CO_2. Capsule thickness in µm (mean ± SD) is noted below each panel. All primary images are at the same magnification; scale bar, 10 µm. For this and other microscopy figures, any region demarcated by a small square is enlarged in the inset at upper right. **(D)** Distribution of normalized capsule thicknesses for the indicated strains. At least 96 cells were measured for each strain as described in the Methods. *, $p<0.0332$; ****, $p<0.0001$ by 2-way ANOVA with Tukey's multiple comparison test; ns, not significant.

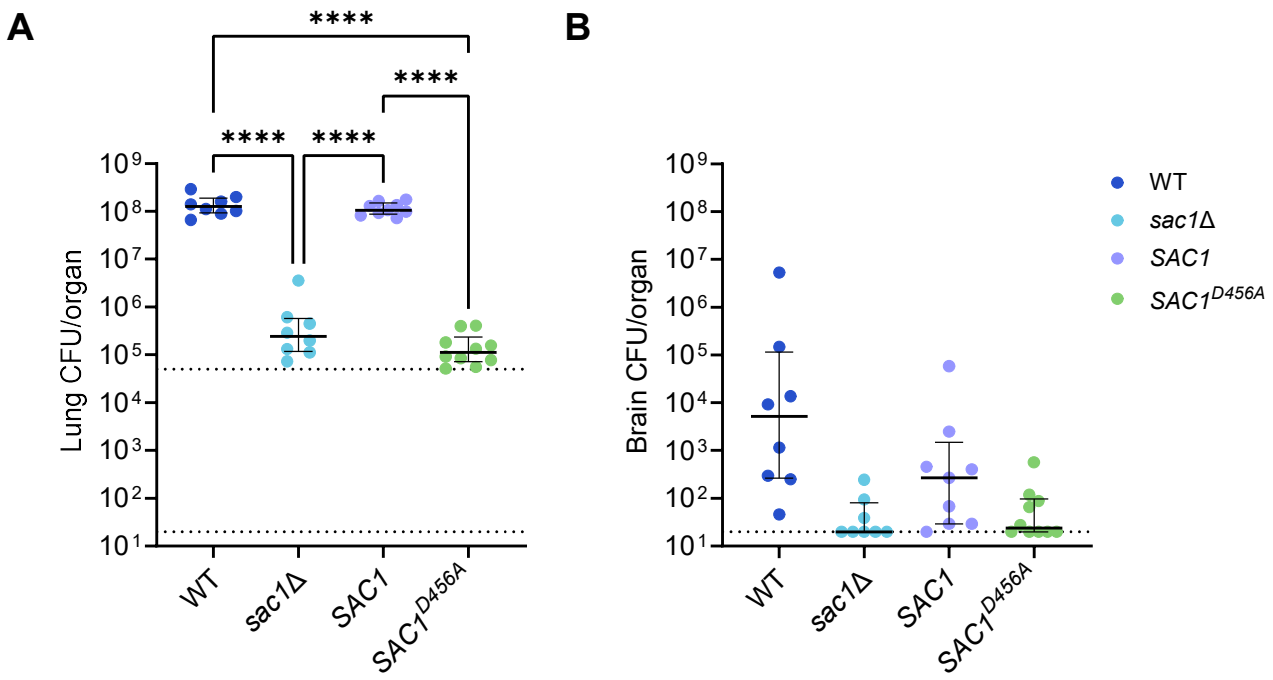

Figure 3. **Sac1 is important for virulence in a mouse infection model. (A)** Lung and **(B)** burden of C57BL/6 mice (groups of 8-10) sacrificed 14 days after intranasal infection with $5x10^4$ fungal cells (upper dotted line). Plots show median (bold black line) with interquartile range. Lower dotted line, limit of detection. Each symbol represents one mouse. ****, $p<0.0001$; comparison with no stars shown are not significant. Significance was calculated using 2-way ANOVA with Tukey's multiple comparison test.

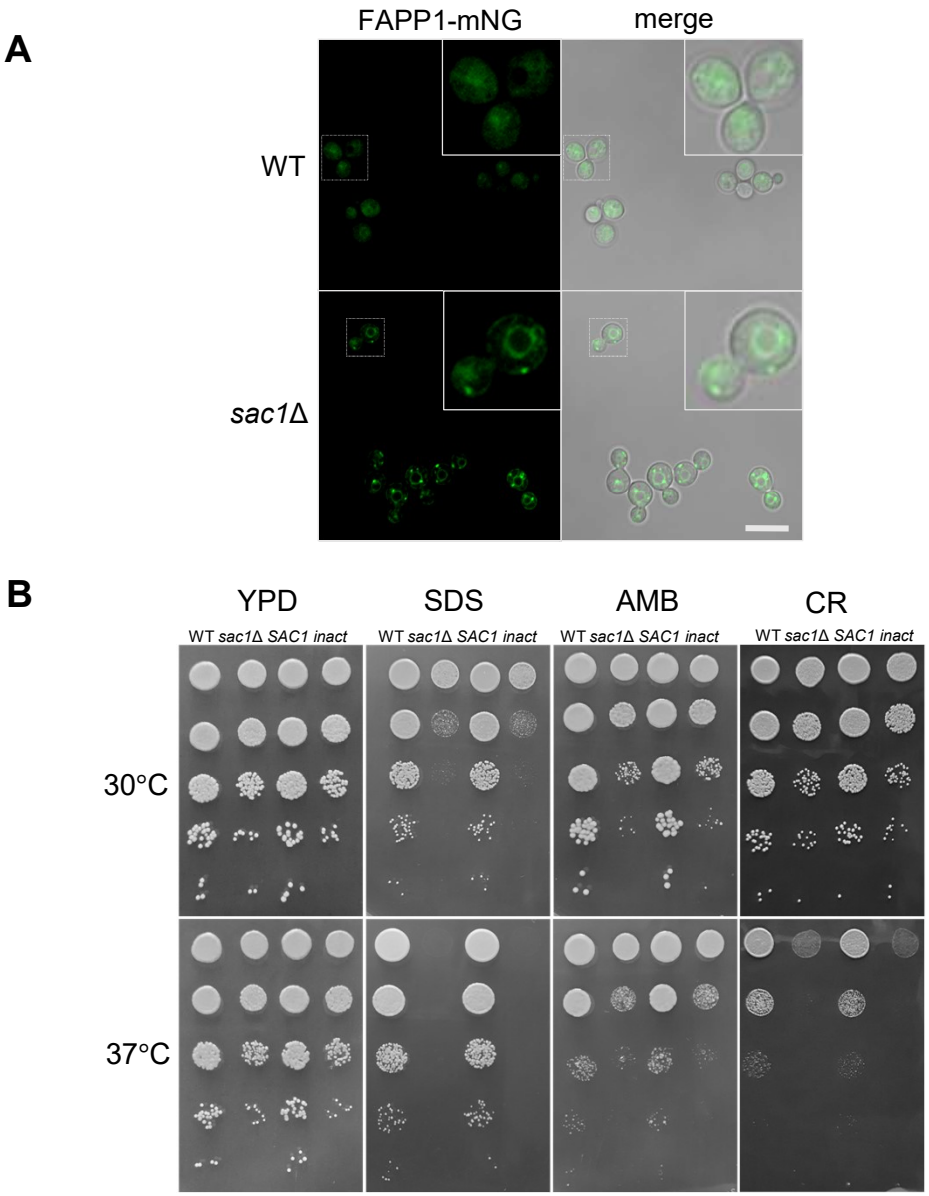

Figure 4. Sac1 regulates substrate distribution and stress sensitivity. (A) FAPP1-mNeonGreen (mNG) localization in cells grown in YPD at 30°C. All primary images are at the same magnification; scale bar, 10 µm. **(B)** Serial 10-fold dilutions of the indicated strains plated on YPD alone or containing 0.01% SDS (SDS), 0.05% Congo Red (CR), or 2 µg/mL Amphotericin B (AMB), incubated at 30 and 37°C. *inact* = *SAC1*^{D456A}.

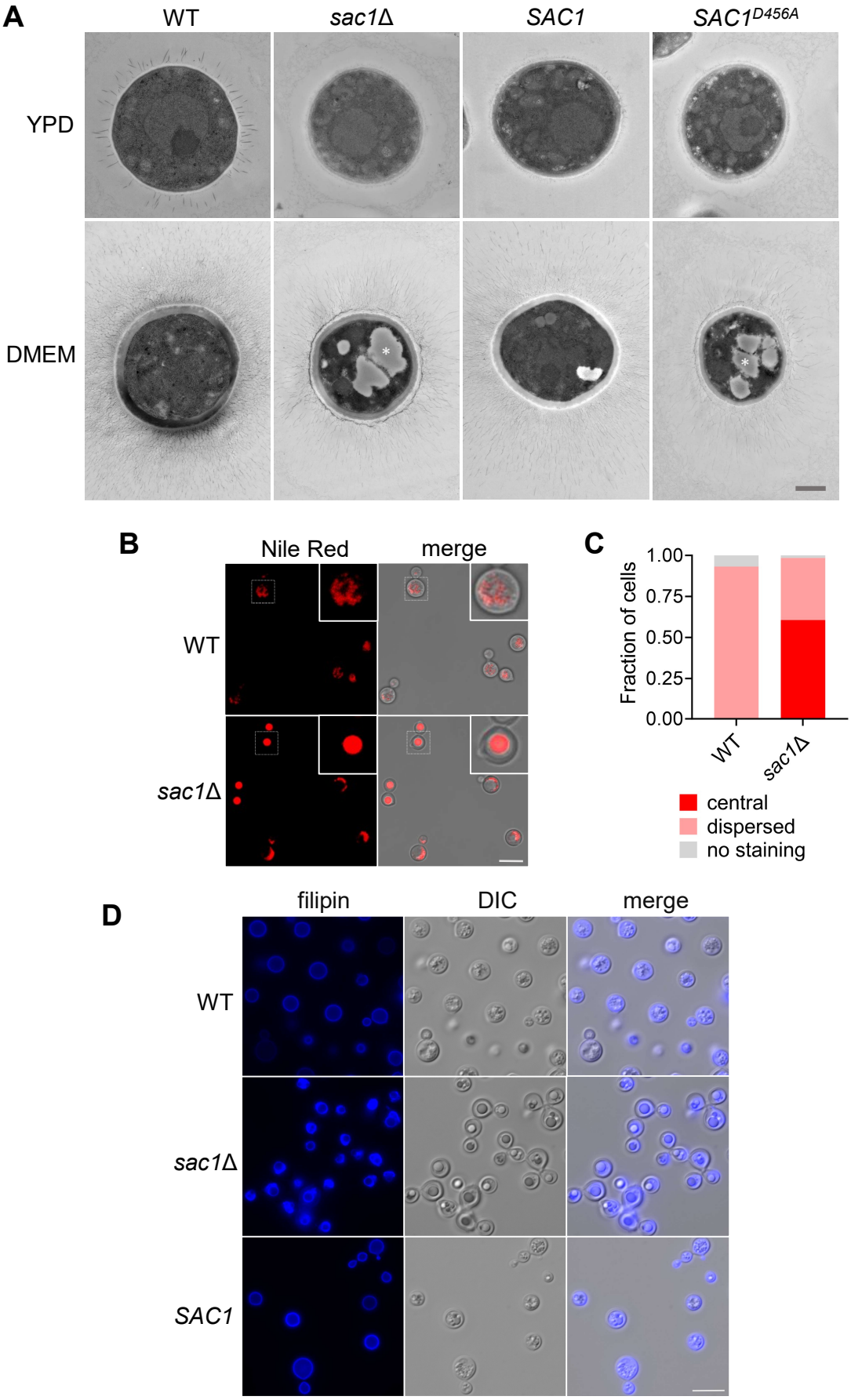

Figure 5. Sac1 is essential for proper lipid trafficking in host-like conditions. (A) Transmission electron micrographs of cells grown in the indicated medium. White asterisks, example lipid droplet structures, likely distorted during sample prep; scale bar, 1 µm. **(B)** Nile Red stain of the indicated strains with **(C)** quantification of the observed staining pattern. **(D)** Filipin staining of cells grown in DMEM. YPD grown cells in Panel A were grown overnight at 30 °C, all other cells were grown for 24 h in DMEM at 37°C with 5% CO_2. Scale bar, 10 µm. All images within each experiment are shown at the same magnification.

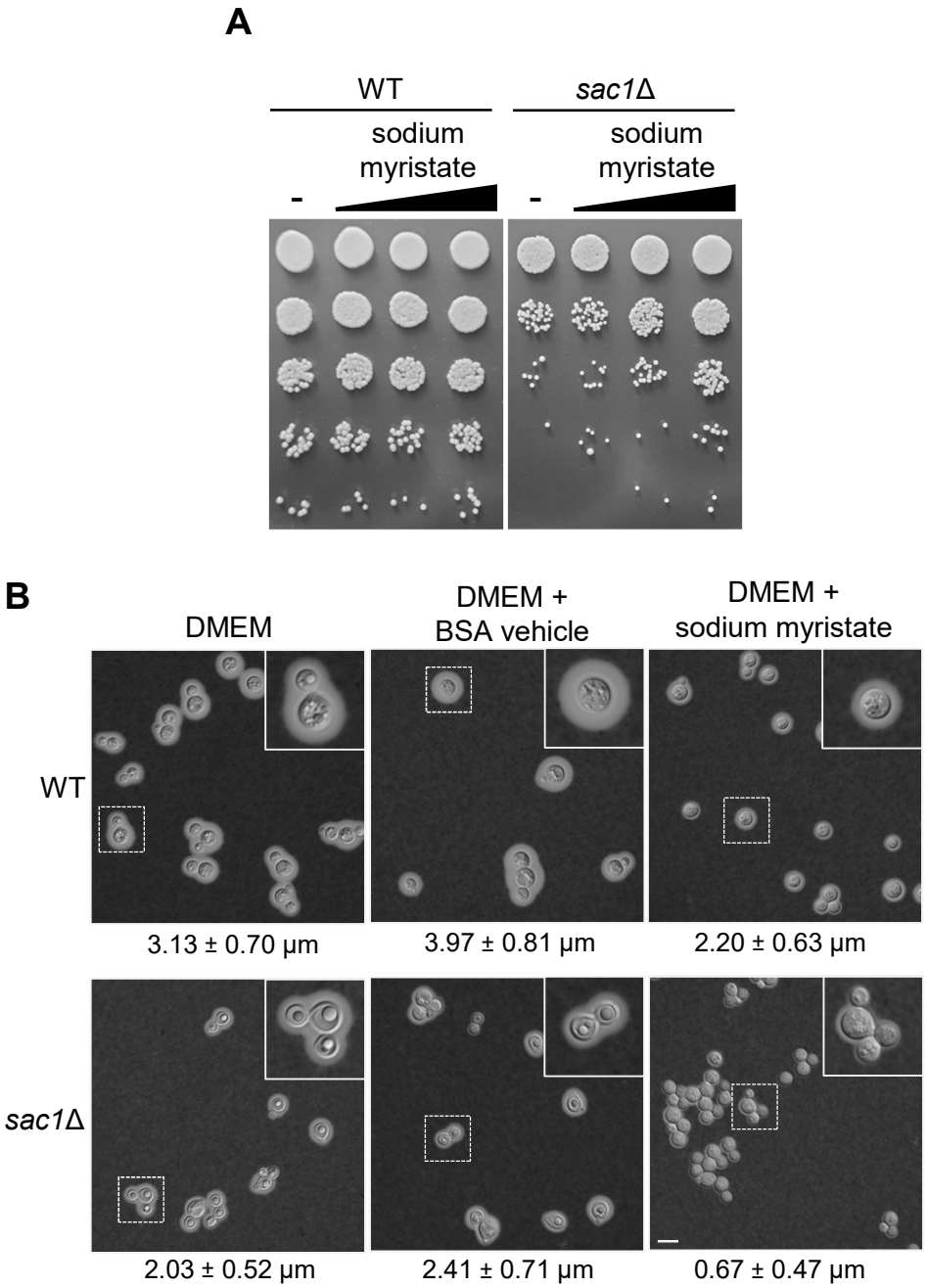

Figure 6. Supplementation with exogenous fatty acid partially restores *sac1*Δ growth and morphology but not capsule biosynthesis. (A) Serial 10-fold dilutions of WT and *sac1*Δ cells grown for 24 hours (at 37°C with 5% CO_2) in DMEM supplemented with BSA alone (-), or with 8, 40, or 200 μM myristic acid conjugated to BSA (increasing amounts indicated by the triangle). **(B)** India ink negative stain of WT and *sac1*Δ cells grown in DMEM at 37°C with 5% CO_2, supplemented as indicated with BSA alone or 200 μM myristic acid conjugated to BSA. Capsule thickness in μm (mean ± SD) is noted below each panel. All primary images are to the same magnification; scale bar, 10 μm.

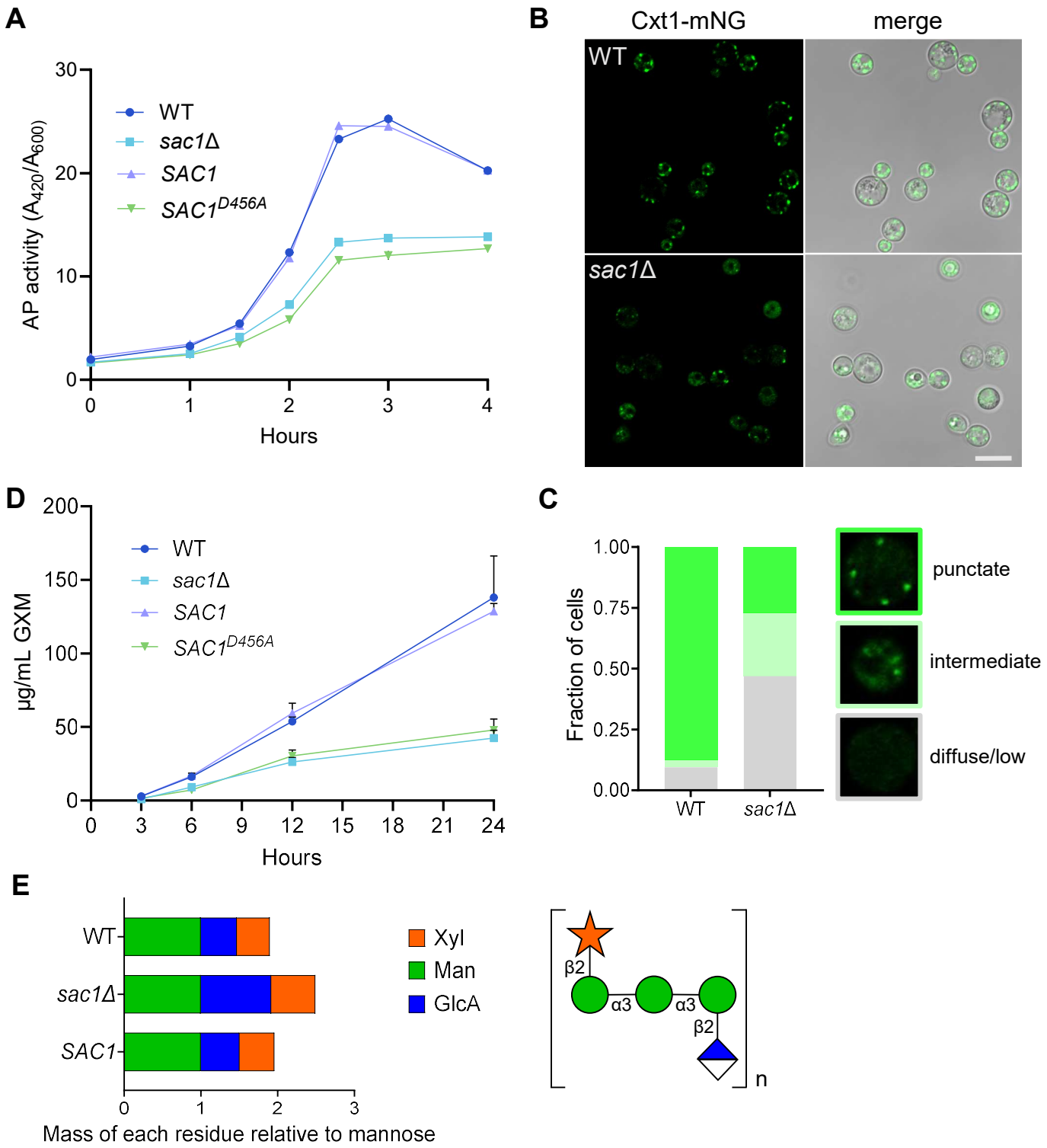

Figure 7. Sac1 controls the secretory pathway to modulate capsule size and composition. (A) Secreted acid phosphatase activity, normalized to cell number, over time after a shift to phosphate-depleted medium. **(B)** Confocal imaging of Cxt1-mNG in the indicated strain backgrounds with **(C)** quantification of observed staining patterns. Punctate: 3 or more puncta present; Intermediate: puncta and diffuse signal; Diffuse/low: diffuse signal or <3 puncta. Images are to the same scale; scale bar, 10 µm. **(D)** Shed GXM quantified by ELISA. For both **(A)** and **(D)**, mean ± SD for one representative experiment of three biological replicate studies is shown. **(E)** Left, GXM composition; right, subunit structure of GXM.

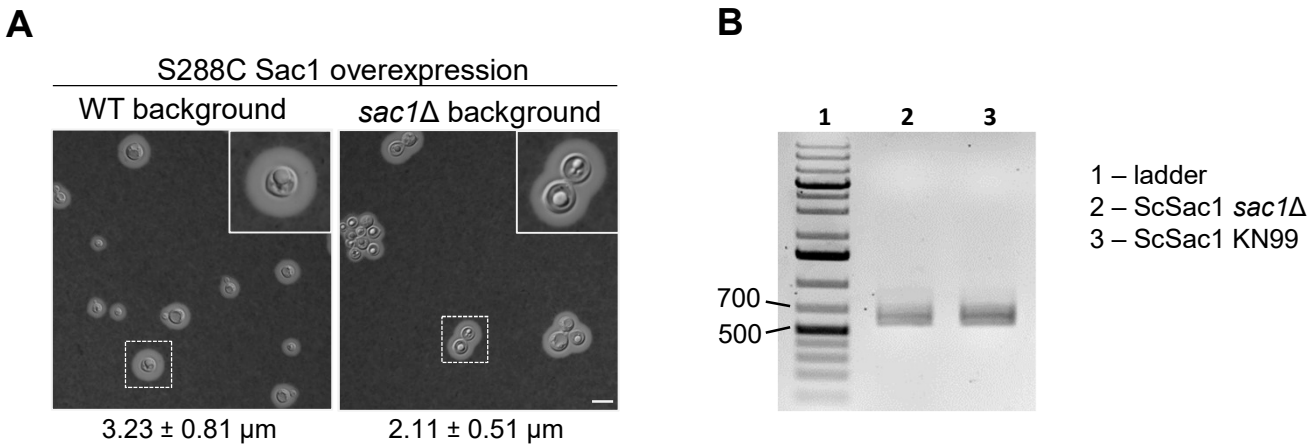

Supplemental Figure S1. Overexpression of the *S. cerevisiae* Sac1 protein in *sac1*Δ does not restore *C. neoformans* capsule synthesis. (A) Negative stain of the indicated strains grown for 24 hours in DMEM at 37°C with 5% CO_2, with the capsule thickness in µm (mean ± SD). Scale bar, 10 µm. **(B)** Amplification of a unique 651 bp region of the S288C Sac1 coding sequence from cDNA generated from fungal cells of the indicated strain grown in YPD shows that the *S. cerevisiae SAC1* gene is expressed in both *C. neoformans* strains.

A

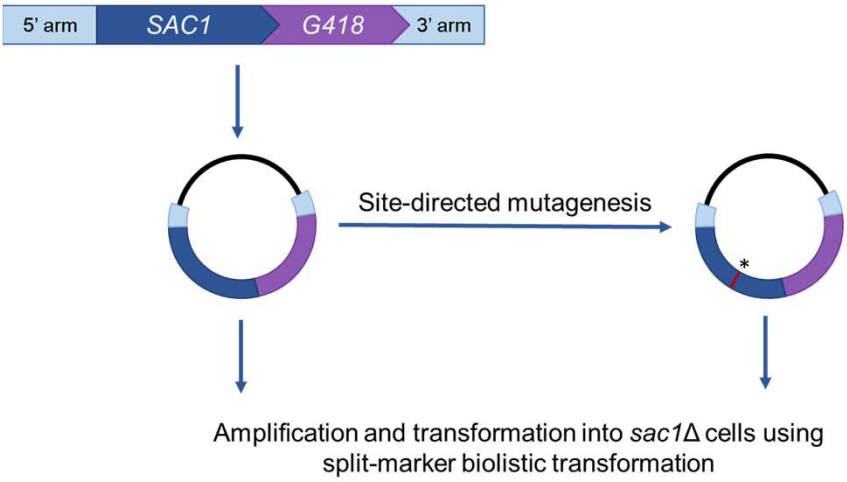

B

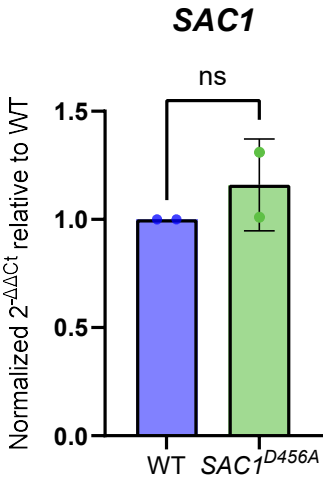

C

```
ATGGCGTTTAATGCTCTACCTGTATGTGACCTTCGCGAAGTGAACTGGCTGCCGCTAACAAGACTTAGCTTCACGAAACC
TTAAACCTCTACGTCTCTCCTACGGCTTACATTTTCGAGCCTGCTTCCTCCAGTGCTGGCCATGTGGGAATCGATGGAAC
TATATTCGTTGATGAAAAGAATGTAAGGGAGAGTATGGTTGTGGACCGTCAGACTGGCCAGATTAGCTTGAGTAGTGAGT
GACAACCCTTGCAATGCGTGGAGCAGAATATCACTGATGCGACAGAACATAACAGCGGCTTCTCATATACCATTTGGAAA
GGAAAAGGTTATTACTTGCTACGGTATTATTGGCATTCTCAGCCTTGCTACTAGTAAGTTTTGTTGCTCCTCAGACACAA
TTGCCCCCTGCTGATTTTGTGCTTTCTAATAGCCGATTTTCTTCTTATTGTCACTTCCCGCTCTCCTTCATGTCGCCTTC
TTTCTCACCCTATCTATCTTGCGAATGATTATCGACTTCTTCCTATTTCCCCTCTGTCTACTTCCTCCGCCATTCTTGAA
CATCCTGTGGAGAAGGAACTCATCTCTCTTGTTGAGCAGGGTCTCAAATCCAGTAAACTCTGGTTCTCGTATGGTTGGGA
CCTTACCAATTCTTTGCAGAGGCAACAAGAAATCGATTTGAAGCTCTCACAGTCCGGAGAACAATGGCCCGCCTGGAGAC
GGGCAGATGAACGTTTCTTTTGGAACAGGTTTCTCATGGACAAGATGATTGACGTGACCGAGAGCGGTGAGGCAGATCTG
AGCCGATTTATCCTTCCTATAATGTACGGCTCTATTGAGCTTCGGTCATCGACTCTTAACTCTCGGGATCTCCTTTTCCT
ACTCATCTCTCGGCGATCTCGTTACCGAGCTGGTACCAGATACTTCACGCGAGGCATCAACCCCTCTGGCCACGTCGCCA
ATTTCAACGAGACTGAGCAAATTGTTATGTATGACCCTATCCCGGAGAACGGAGAAGCCTACGGAAGGGGAAGGGTAGAC
GGTAGGGAAAGGCTGAGCTTTGTGCAGACAAGAGGGAGTGTTCCGCTATTCTGGGCCGAGGTCAACAACTTGAGGTACAA
GCCCGATTTGCAAATTATGGATTACACTGAGACGGTGAGTGAATTGTATTGAAAGGCATGACATGTCCTGACAATGAATT
AGCCTCAAGCTCTCAAAGCACATCTCAACAGTATGATTAAGACCTATGGCCATACATATCTTGTGAATCTTGTAAATCAA
AAGGGACACGAACAACCTGTCAAGGAAGCTTTTGAGCGCTACATGTCCCTTGTCGCCTCATCCGACCCGTCCATTCAGGA
GAAGGCTCACTACCTCTACTTTGACTTTCACCACGAATGCAAAGGTCTAAGGTTTGACCGAATTTCCCTTTTGGTCGAGA
AGCTTGCGACAGCACTTGAGGATATGAGCTGGTACCATTCTGTCAACCCCGACTCGTCAACCTATGCTCTCTTGCAACCA
AACTCTGCAGACACCCAGGTACTTACTAAGCAAACGGGCGTCGTCAGAACCAACTGTATGGCGTGTCTAGACAGGACCAA
TGTCGCACAAGCGGCTCTGGCTAGATGGGTTTTGAACCGGCAATTAAGGAAGGTCGGGATCCTGAGCGTGAAGGAAGGTG
TGGAGGATCACGAAGAGTTTATGATTATGTTCCGGAATGGTACGTGCTTTTCATTTTGACTAGAAATTAGACTAACTTGA
GAAAATAGTGTGGGCCGATCATGGTGACACCGTCTCCCGAGCTTATGCAGGAACTGGTGCTCTCAAATCCGACTTTACTC
GTACCGGTAAACGATCCAAGGAGGGTCTCTTGGAAGATGGTTACAAAAGCGTGATGAGATACTTTAGGAATAACTTCTTC
GATGGCGATCGTCAGGTTAGTCCCTACTGTTGTGAGCTGAGAGAGACATCTGACCGGAGAACAGGATGGTTTTGATATTC
TAACTGGAGCATGGGTAGCCCAAAGGGGTGGCATTCCTCCATTGACTGATACAAGACCTCTTATCATGCGCTCGGTAAGT
CCATGGTTTGTCCGACTAATGTTGACCCGAGAAGATGCCGTACATACTGGCGTTTGCTCTCACAATGATCACCGCAGCTC
TCACATTGCCACGAACCTCGGAGATGTCCATATATTCCTTCCTCGTCCTTTGGTTCTTCCTTGCATTCTTCTCAGGAAGT
TATATTTGGGGCAATGTAAGTTATTTTCTTCTTTCATATATTGACTTTGGCCGTTGACCGCCATTTGTCACTCTTAGGGT
ACATCATACGTCTCCTGGCCGCGTTTGAACCCTCCTCTAGAAATTCTCTCTTACTCTGGACCGGGTCACCGCTCTCCGGT
CCGCGGTCGAGGGATGTCGTTCGCAGCCATTGTGCCCCTGTTCGATCGTCGACGCCAAAATGGTCCTGGAGCTGGCGTAC
TTGGTGCCACCGGCGGCTTCGGAGGAAGGAACGATGGAAGACCTGCAATGTATAAGATGGAGGAGTCGGAGTTGGGGAGG
AGGAAGGGTGCGTTGATTGATTAA
```

Supplemental Figure S2. Construction and validation of the *SAC1D^{456A}* strain. **(A)** Strain construction strategy for *SAC1* complement and *SAC^{D456A}* inactivated complement strains. **(B)** Normalized expression of *SAC1* in WT and *SAC1^{D456A}* cells grown for 24 hours in DMEM at 37°C with 5% CO_2. **(C)** Nucleotide sequence of *SAC1^{D456A}*. Red, nucleotide differences from WT *SAC1*.

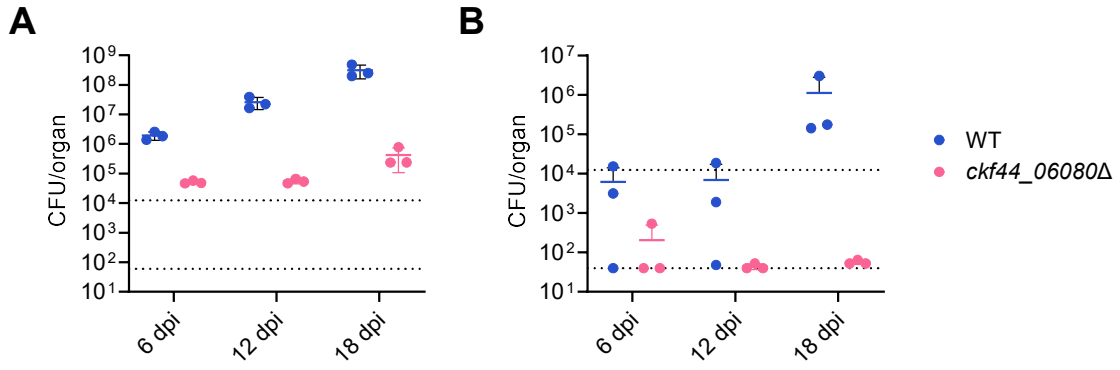

Supplemental Figure S3. Cells lacking functional Sac1 have reduced virulence. (A) Lung and **(B)** brain burden of C57BL/6 mice sacrificed at the indicated days post infection (dpi) with 1.25×10^4 fungal cells of *ckf44_06080*Δ from the Madhani *C. neoformans* deletion collection. Upper dotted line, inoculum. Lower dotted line, limit of detection. Each symbol represents one mouse.

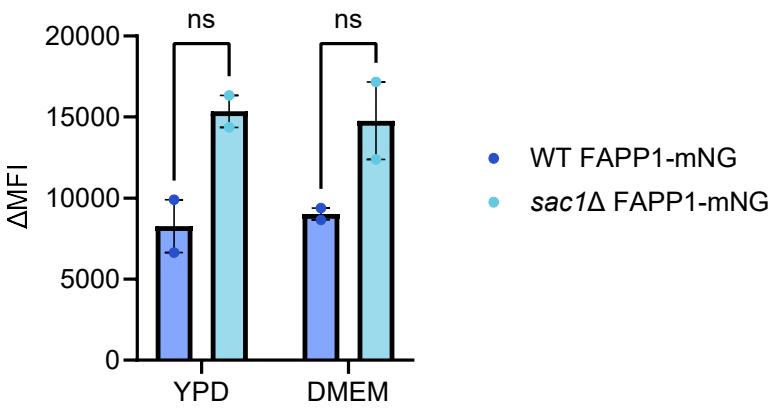

Supplemental Figure S4. PI4P content of WT and *sac1*Δ strains. Difference in median fluorescence intensity between FAPP1-mNG expressing and control cells (ΔMFI) in WT and mutant backgrounds, grown in the indicated medium. ns, not significant by unpaired t test.

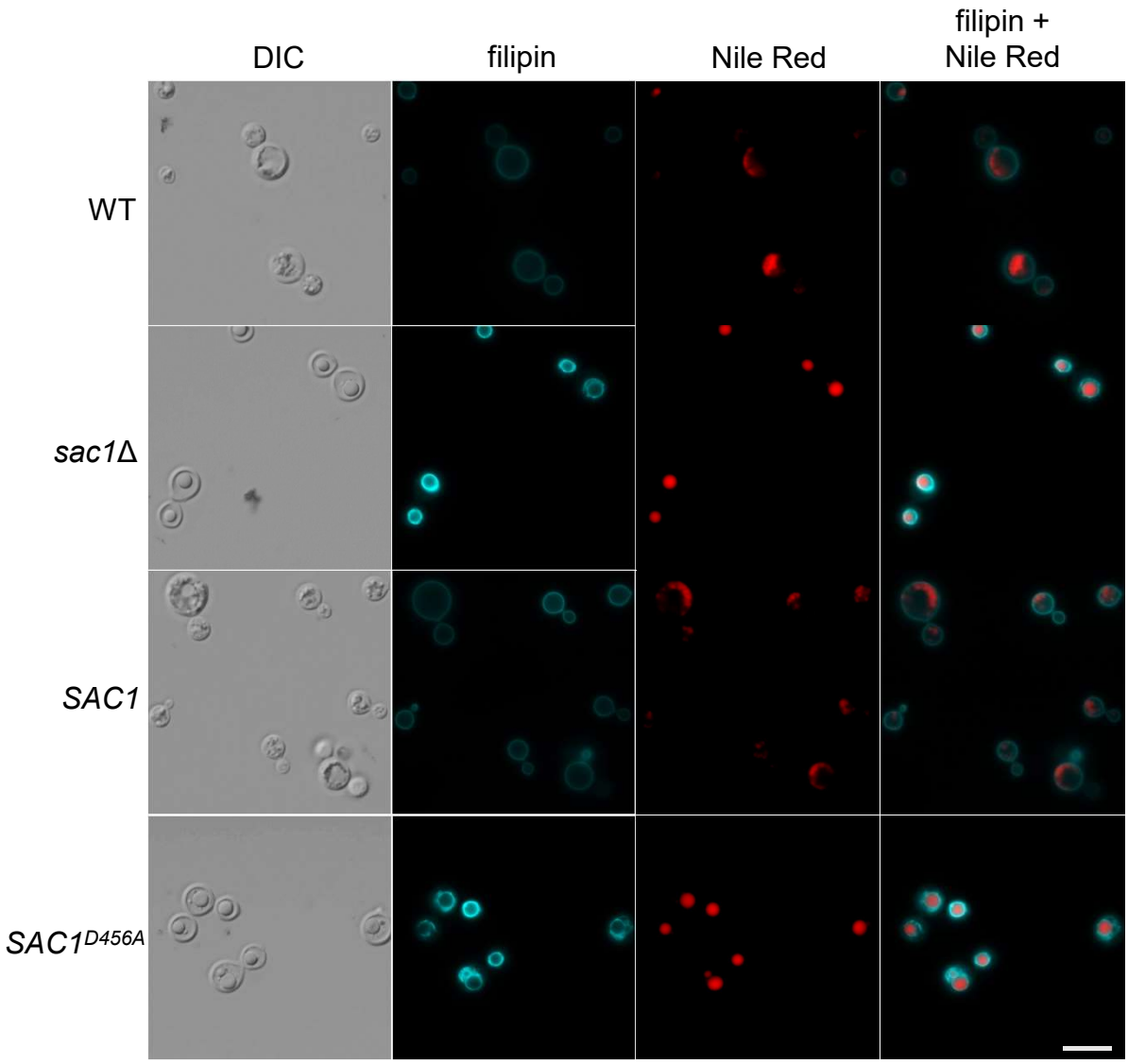

Supplemental Figure S5. Dual staining with filipin and Nile Red. All cells were grown in DMEM for 24 hours at 37°C with 5% CO_2. DIC, Differential interference contrast. Scale bar, 10 µm.

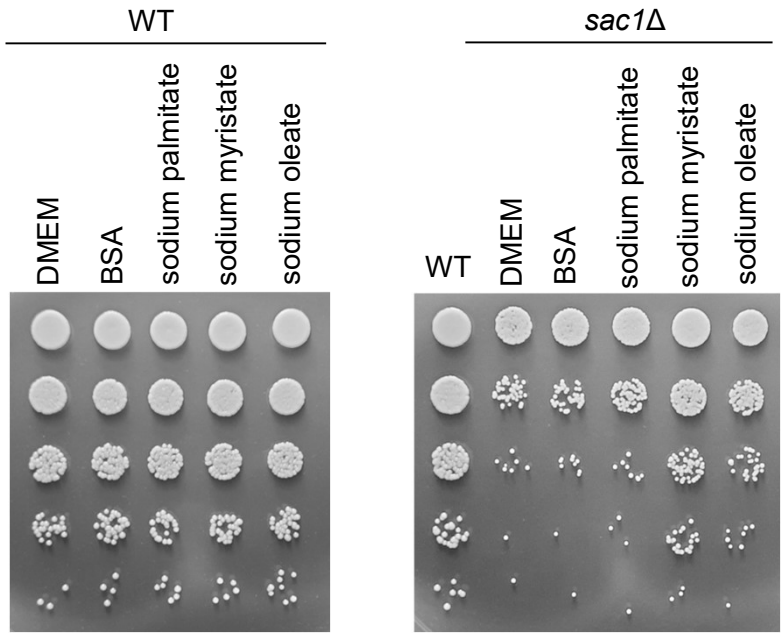

Supplemental Figure S6. Supplementation with exogenous fatty acids partially restores growth of *sac1*Δ cells. Serial dilutions of (left) WT or (right) *sac1*Δ cells grown for 24 hours in DMEM alone, DMEM supplemented with BSA, or DMEM with 100 μM of the indicated fatty acid sodium salt conjugated to 0.4 mg/mL BSA.

Residue	WT #1	*sac1*Δ #1	WT #2	*sac1*Δ #2	*SAC1* #2
Terminal Xylopyranosyl residue (t-Xyl)	12.0	19.7	10.4	16.2	11.1
Terminal Mannopyranosyl residue (t-Man)	1.3	0.3	0.3	0.3	0.4
Terminal Glucopyranosyl uronic acid residue (t-GlcA)	17.9	15.4	19.1	16.2	18.2
3-linked Mannopyranosyl residue (3-Man)	29.9	23.3	27.8	21.1	30.6
2,3-linked Mannopyranosyl residue (2,3-Man)	36.0	38.5	37.5	42.8	34.9
2,3,4-linked Mannopyranosyl residue (2,3,4-Man)	2.9	2.8	4.9	3.5	4.8

Supplemental Table S3. Linkage analysis of independently isolated WT, sac1Δ, and *SAC1* strains. Values are percent area of relevant residue peaks. Numbers in header row refer to independently isolated samples.